Title

Examining Alzheimer's Disease modifiable risk factors: Impact of physical activity and diet on neuroanatomy and behaviour in mouse models

Cindy L. García[1,2¶*], Chloe Anastassiadis[1,2,3¶], Mila Urosevic[4], Megan Park[2], Daniel Gallino[2], Gabriel A. Devenyi[2,5], Stephanie Tullo[2], Yohan Yee[6], M. Mallar Chakravarty[2,5*]

[¶] These authors contributed equally to this work

[1] McGill University - Integrated Program in Neuroscience, Montreal, QC, Canada

[2] Cerebral Imaging Centre - Douglas Mental Health University Institute, Montreal, QC, Canada

[3] Tanz Centre for Research on Neurodegenerative Diseases, Toronto, ON, Canada

[4] Biological and Biomedical Engineering, McGill University, Montreal, QC, Canada

[5] Department of Psychiatry, McGill University, Montreal, QC, Canada

[6] Cumming School of Medicine, Department of Radiology, University of Calgary, Calgary, AB, Canada

[*] Corresponding authors:

E-mail: cindylucerogarcia@gmail.com (CLG), mallar.chakravarty@douglas.mcgill.ca (MMC)

Abstract

Dementia is a global public health challenge, with obesity emerging as an important modifiable risk factor. Here, we examined whether lifestyle interventions can mitigate the effects of diet-induced obesity on body weight, behaviour, and brain anatomy in mouse models. Using a longitudinal design, wild-type and triple-transgenic (3xTgAD) mouse models of Alzheimer's disease were exposed to a high-fat diet and assigned to one of three interventions: voluntary physical activity, a low-fat diet, and their combination. A high-fat diet significantly increased body weight and induced widespread neuroanatomical changes, with effects modulated by sex and genotype. The combined intervention led to significant weight loss in males of both genotypes. Neuroanatomical analyses revealed that a high-fat diet significantly reduced hippocampal and cerebellar volumes in wild-type mice but had a less pronounced effect on 3xTgAD mice; nevertheless, interventions, particularly the combined approach, increased localized brain volumes in these regions regardless of genotype.

Multivariate integration of behavioural and neuroanatomical measures identified a brain pattern linking hippocampal and cerebellar volumes to intervention and behavioural performance. Spatial gene enrichment analysis of this pattern identified biological processes, including glucose homeostasis, as potential biological mechanisms underlying intervention effects. Overall, these findings suggest that voluntary physical activity and a low-fat diet can modulate brain structure and behaviour, partially counteracting the effects of a high-fat diet, and potentially recruiting biological processes that may support brain health.

45 # Introduction

46

47 Dementia is characterized by severe cognitive decline that impacts the ability to perform tasks
48 related to daily living (Gale et al., 2018), and it is projected to affect ~78 million people worldwide
49 by 2030 (World Health Organization, 2021). Although increasing life expectancy contributes to
50 the growing prevalence of dementia, age remains the strongest risk factor for neurodegenerative
51 disorders (Niccoli and Partridge, 2012). Importantly, dementia is recognized as a condition that
52 develops over several decades before clinical diagnosis (Iturria-Medina et al., 2016). Consistent
53 with this extended preclinical phase, approximately 15% of dementia cases are attributable to mid-
54 life (45-65 years) modifiable factors such as hypertension, alcohol consumption, and obesity
55 (Livingston et al., 2020).
56 Strategies aimed at addressing obesity are acknowledged as effective approaches for preventing a
57 range of chronic diseases, such as cancer, diabetes, and cardiovascular conditions (Knowler et al.,
58 1995; Rexrode et al., 1996; Tubiana, 1999). Notably, the Alzheimer's Association and the Lancet
59 Commission on Dementia report that obesity during mid-life increases the risk of cognitive decline
60 and dementia, whereas this risk is reduced when obesity occurs later in life (Baumgart et al., 2015;
61 Livingston et al., 2024). Several studies have linked weight maintenance and physical activity with
62 a lower risk of developing dementia (Albanese et al., 2017; Hörder et al., 2018; Huang et al., 2022;
63 Zotcheva et al., 2018). For example, combining physical activity with a Mediterranean diet
64 effectively lowers the risk of developing Alzheimer's Disease (AD), the most common form of
65 dementia (Scarmeas et al., 2009). Conversely, diets high in saturated fats increase inflammatory
66 markers such as interleukin-6 (Milanski et al., 2009), which has been implicated in the

67 pathogenesis of AD (Khan et al., 2020), highlighting the importance of dietary factors in dementia
68 prevention.
69 Only a few studies have examined the neuroanatomical effects of obesity and intervention
70 strategies. For instance, it has been shown that obesity is associated with lower gray matter
71 volumes in regions including the frontal gyri, insula, and cerebellum (García-García et al., 2019;
72 Gómez-Apo et al., 2021). In previous work from our laboratory, an obesity-inducing high-fat diet
73 led to widespread morphological changes, including a decline in hippocampal volume in the triple
74 transgenic mouse model of Alzheimer's disease (3xTgAD) (Rollins et al., 2019). In contrast, other
75 studies have found larger volumes in the hippocampus and cerebellum related to physical activity
76 (Brown et al., 2022; Cahill et al., 2015; Raji et al., 2024).
77 Despite the strong epidemiological evidence linking mid-life obesity to dementia risk, evaluating
78 the effectiveness of intervention strategies in humans remains challenging due to the need for long-
79 term follow-up (Livingston et al., 2024). This emphasizes the importance of experimental models
80 that allow controlled research to understand how risk factors and interventions affect the brain.
81 The present study builds upon our previous work (Rollins et al., 2019) to investigate the effects of
82 three intervention strategies: physical activity, low-fat diet, and the combination of both, in the
83 3xTgAD mice and their wild-type (WT) counterparts, after receiving a high-fat diet. Animals were
84 studied longitudinally from two to six months of age; a period that corresponds to late adolescence
85 and early adulthood in humans (Cottam et al., 2025). This interval allows for the assessment of
86 intervention efficacy during the initial stages of amyloid and tau development, which is
87 accompanied by cognitive impairments in 3xTgAD mice (Billings et al., 2005).
88 During this period, mice underwent an interleaved protocol. After being maintained on a standard
89 diet for two months, they were switched to a low-fat or high-fat diet until four months of age,

followed by interventions from four to six months. We collected weekly body weight measurements and acquired T1-weighted (T1-w) magnetic resonance images (MRI) of mice at two, four, and six months of age. Behavioural tests (Morris water maze and novel object recognition tests) were conducted after the last MRI scan. We related voxel-wise structural brain changes to behavioural outcomes using partial least squares analysis (PLS), a multivariate method that identifies patterns of covariation between the two datasets without imposing prior neuroanatomical assumptions. We then applied Spatial Gene Enrichment Analysis (SGEA) to gain insight into the potential biological mechanisms underlying the PLS-derived brain pattern. This approach uses spatially resolved gene expression data from the Allen Mouse Brain Atlas (Lein et al., 2007) to identify genes whose expression patterns correlate with the observed brain pattern, and to determine which biological processes are enriched among these genes. The aim of this study was to determine whether lifestyle interventions, including physical activity and a low-fat diet, mitigate the effects of a high-fat diet on body weight, behaviour, and brain anatomy in wild-type and 3xTgAD mice. Our findings support this aim, demonstrating that interventions attenuated high-fat diet effects in a genotype-, sex-, and outcome-dependent manner.

Results

Raw data and statistical maps generated during this study are available in the repository listed under the "Data and materials availability" section.

Experimental groups and study timeline

A detailed description of group composition, sex ratios, and diets is provided in Materials and Methods (section 'Experimental design'). Briefly, all mice were maintained on a standard diet (4% kcal from fat) from birth to 2 months of age (initial N = 165, Fig 1A). From 2-4 months, mice were switched to either a low-fat (10.5% kcal from fat) or a high-fat diet (60% kcal from fat). The low-fat diet is ingredient-matched to the high-fat diet, allowing macronutrient-specific comparisons. WT and 3xTgAD mice that remained on a low-fat diet throughout the experiment are referred to as Controls (WT_Control, Tg_Control). From 4-6 months of age, mice previously exposed to the high-fat diet were assigned to one of four conditions: 1) continuation of the high-fat diet with no further intervention (WT_HighFat, Tg_HighFat); 2) a low-fat diet intervention (WT_Diet, Tg_Diet); 3) access to a wheel for voluntary physical activity while remaining on a high-fat diet (WT_Exercise, Tg_Exercise); or 4) a combined low-fat diet and voluntary exercise intervention (WT_Both, Tg_Both). Body weight was measured weekly from 2 months of age until the end of the experiment. Longitudinal T1-w MRI were acquired at 2, 4, and 6 months of age (100 μm isotropic resolution, Bruker 7T). Following the last scan, novel object recognition and Morris water maze tests were performed to assess intervention effects on memory.

Intervention strategies affect the body weight of mice

Mice were weighed weekly after the change in diet (from standard diet) at two months of age and until the end of the experiment (final N = 156 mice, 18 measures of weight per mouse). To analyze the weight changes per group following intervention onset (Fig 1B), we fit a linear mixed effects model (LME) including a four-way interaction between time (in weeks), intervention, genotype, and sex as fixed effects, along with a random intercept and slope for time at the individual level, to account for repeated measurements and individual variability in weight change over time ($Weight \sim Week*Intervention*Genotype*Sex + (Week|ID)$). Because higher-order interaction terms are difficult to interpret directly, given that the effect of a variable depends on the values of others (Busenbark et al., 2022), we computed model-based marginal comparisons (Arel-Bundock, 2025). These estimates quantify the expected change in body weight (grams/week) for each intervention, genotype, and sex. This approach enables direct comparison of rates of weight gain or loss across intervention groups (see Statistical Analyses, section 'Weight and behaviour'). Marginal comparisons (Fig 1C) revealed that during the intervention period (week ≥ 8), mice maintained on a high-fat diet continued to gain weight at a significant rate across genotypes and sexes (0.85 - 1.07 g/week, $p < 0.001$). Mice in the control groups also kept gaining weight at lower rates than those on a high-fat diet (0.39 - 0.46 g/week, $p \leq 0.006$), with 3xTgAD males showing weight stabilization (rates of weight change not significantly different from zero). Interventions differentially altered weight trajectories depending on sex and genotype. Mice receiving a Diet intervention showed weight stabilization. Exercise alone resulted in varied outcomes. WT males (0.68 g/week, 95% CI [0.45, 0.92], $p < 0.001$) and 3xTgAD females (1.05 g/week, 95% CI [0.74, 1.36], $p < 0.001$) continued to gain weight despite access to a wheel while maintained on a high-

156 fat diet. In contrast, WT females and 3xTgAD males displayed weight stabilization. The combined
157 intervention (Both) resulted in significant weight loss in males of both genotypes (WT: -0.38
158 g/week, 95% CI [-0.63, -0.121], p = 0.004; 3xTgAD: -0.52 g/week, 95% CI [-0.85, -0.19], p =
159 0.002), while females of both genotypes exhibited weight stabilization. Taken together, these
160 results point to a sex- and genotype-dependent modulation of weight trajectories in response to
161 intervention.
162

163 **Volumetric effects of genotype, high-fat diet, and interventions**

164

165 To assess the effects of genotype, high-fat diet, and interventions on brain anatomy, we applied a
166 hierarchical LME model to the 182 regional volumes derived from the MAGeT brain segmentation
167 algorithm (Chakravarty et al., 2013) using the Dorr-Steadman-Ullmann-Richards-Qiu-Egan
168 (DSURQE) mouse brain atlas (Dorr et al., 2008; Richards et al., 2011; Steadman et al., 2014;
169 Ullmann et al., 2013), as described in Materials and Methods, section 'Volumetric analysis'. We
170 used brain images collected at 2, 4, and 6 months of age. The model included an interaction
171 between group and age, modeled as a quadratic term to account for nonlinear trajectories (Fjell et
172 al., 2010), sex as an independent variable, and a random intercept per mouse (model: *Volume* ~
173 *Group**poly(*Age*,2) + *Sex* + (*1*|*ID*)). All model outputs were corrected for multiple comparisons
174 at a 10% False Discovery Rate (FDR) threshold (Benjamini and Yekutieli, 2001).
175 Comparing 3xTgAD and WT mice under control conditions revealed widespread volumetric
176 differences, as detailed in the Supplementary Results (section 'Volumetric analysis'). However,
177 when examining the impact of the high-fat diet and subsequent interventions, significant

178 volumetric changes were restricted to WT groups. In the 3xTgAD mice, these regional volumetric
179 measures showed limited detectable changes (Supplementary Figs S1-S3).
180 These findings suggest that while regional volumetric analysis is highly effective for capturing
181 global genotype differences, it may be less sensitive to more subtle changes, such as early atrophy
182 or partial recovery in 3xTgAD mice. This motivated our subsequent use of Deformation-Based
183 Morphometry (DBM), a voxel-wise approach capable of identifying localized structural shifts that
184 may be obscured when averaging across entire anatomical regions (Germann et al., 2025; van Eede
185 et al., 2013).
186

187 Deformation-based morphometry identifies similar patterns of local 188 brain changes

189

190 To capture changes without relying on predefined neuroanatomical boundaries, we performed
191 voxel-wise DBM analysis (see Materials and Methods, section 'Deformation-Based Morphometry
192 analysis'). DBM quantifies local structural differences by measuring the deformations required to
193 align individual brain images to a common population template. These voxel-wise deformations
194 are summarized by the Jacobian determinant, which reflects local volume expansion (positive
195 values) or contraction (negative values) relative to the population average (Chung et al., 2001).
196 DBM has been previously applied by our group to study morphological changes in the 3xTgAD
197 (Kong et al., 2018), 3xTgAD receiving a high-fat diet (Rollins et al., 2019), models of
198 synucleinopathy (Tullo et al., 2024), and neurodegeneration in Parkinson's and frontotemporal
199 dementia (Bussy et al., 2023; Tullo et al., 2025).

LME models were fitted at each voxel using the log-transformed Jacobian determinant as outcome, with an interaction between group and age in days (modeled as a quadratic polynomial), and sex, along with a random intercept for each mouse (model: *log-Jacobian* ~ *Group**poly(*Age*,2) + *Sex* + (*1*|*ID*)). Data from all time points were included, and results were corrected for multiple comparisons with FDR at a 10% threshold. While the quadratic interaction term was included to detect potential non-linear trajectories, these effects were limited to highly localized cortical areas and the olfactory bulbs (Supplementary Fig S4). In contrast, the linear term of the interaction captured widespread changes in brain volume over time (Fig 2). These linear changes are most relevant to our hypothesis, which anticipated gradual neuroanatomical changes driven by a high-fat diet and the subsequent interventions.

DBM results are summarized in Fig 2. The comparison between Tg_Control versus WT_Control (genotype effect) revealed widespread significant differences in the cerebellum, hippocampus, caudoputamen, cortex, and olfactory bulbs. High-fat diet effects (comparison of Tg_HighFat and WT_HighFat against their controls) were again found in the cerebellum as well as the hippocampus and caudoputamen, with no major voxel-wise effects detected in 3xTgAD mice, consistent with the volumetric analysis. This suggests that the high-fat diet effect is modulated by genotype, with WT mice exhibiting greater sensitivity.

However, while the effects of a high-fat diet are less prominent in the 3xTgAD mice, the subsequent voxel-wise analysis of intervention effects revealed localized structural growth that was previously obscured in the regional volumetric analysis.

Relative to mice fed a high-fat diet, the dietary intervention (Fig 2, 'Diet intervention effect') was associated with a significant volume increase within cerebellar regions in both genotypes, reaching control-like values, whereas physical activity (Fig 2, 'Exercise intervention effect') promoted

volume growth in hippocampus and cerebellum. The combined intervention (Fig 2, 'Effect of combined intervention effect') resulted in significant structural growth in the cerebellum of both genotypes and in the hippocampus of 3xTgAD mice. No significant sex differences were observed across any comparisons. Evidence regarding the directionality of these structural changes is provided in the following section, which illustrates the significant peak voxel trajectories (Figs 3-5 and Supplementary Figs S5-S6).

In summary, DBM analysis demonstrates that genotype-driven differences follow a consistent spatial signature involving the cortex, cerebellum, and hippocampus, a pattern that is partially mirrored in WT mice exposed to a high-fat diet. Importantly, by bypassing the constraints of predefined anatomical boundaries, DBM successfully captured intervention-related structural preservation in 3xTgAD mice that were not detectable using regional volumetry.

Peak-voxel trajectories reveal that intervention strategies influence local brain structure

Thus far, both volumetric and DBM analyses revealed statistical effects driven by genotype, high-fat diet, and intervention strategies. To characterize the directionality of the volumetric changes underlying these effects, we selected peak voxels to examine voxel-wise trajectories. Peak voxels were defined as those with the highest t-values from the DBM statistical maps that survived a 10% FDR threshold.

In Fig. 3, the left panels display the statistical maps overlaid on the population average, along with the t-value and coordinates of the selected peak voxel. The middle panels show longitudinal trajectories expressed as percent volume change from baseline. The right panels display the percent

246 volume change reached at the end of the intervention period (6 months of age), highlighting the
247 group differences observed at the final time point.
248 We first illustrate the genotype effect by comparing Tg_Control and WT_Control at significant
249 peak voxels identified in two brain regions: the hippocampus (Fig. 3A) and the cerebellum (Fig.
250 3B). In the hippocampus, by the final time point (right panels), Tg_Control shows minimal
251 volumetric change from baseline (~2%), which is significantly lower than the ~20% increase
252 observed in WT_Control. In the cerebellum, Tg_Control exhibits a significant reduction in volume
253 (~ -4%), whereas WT_Control shows an average increase of ~8% at the same voxel. These patterns
254 are consistent with the volumetric results (Supplementary Figs. S1B–S1C). Trajectories for the
255 same voxel are also shown for the other intervention groups for visual comparison.
256 To examine the effect of a high-fat diet, we identified significant peak voxels showing differences
257 between HighFat and Control groups. In WT mice, a peak voxel in the hippocampus (Fig. 4A, top
258 panel) shows that WT_Control mice exhibit ~20% volume growth from baseline by the final time
259 point, whereas WT_HighFat mice remain close to baseline, indicating markedly reduced growth.
260 In the cerebellum (Fig. 4B, top panel), WT_HighFat mice display an ~7% reduction in volume
261 relative to baseline, contrasting with the modest volume increase observed in WT_Control mice.
262 In 3xTgAD mice, a significant peak voxel in the cerebellum (Fig. 4A, bottom panel) reveals
263 divergent trajectories between Tg_Control and Tg_HighFat groups, with Tg_HighFat mice
264 showing a pronounced decline in volume across time. Together, these results indicate that a high-
265 fat diet alters longitudinal volume trajectories, with particularly pronounced effects observed in
266 WT mice.
267 Lastly, we report peak voxels identified for each genotype under the combined intervention (Fig.
268 5). In WT mice, a significant peak voxel in the cerebellum (Fig. 5A, top panel) shows that

269 WT_Both mice exhibit greater percent volume change from baseline (~10%) than WT_Control
270 and differ significantly from WT_HighFat, which shows a decline in volume. This pattern is
271 consistent with enhanced regional volume growth under the combined exercise and diet
272 intervention.
273 In 3xTgAD mice, a peak voxel in the hippocampus (Fig. 5A, bottom panel) reveals a similar
274 pattern: Tg_Both mice show greater percent volume change from baseline (~10%) than
275 Tg_Control, indicating localized volume growth under the combined intervention despite the
276 absence of a detectable high-fat diet effect in this region.
277 Additional peak voxel trajectories for diet and physical activity groups are shown in
278 Supplementary Figs. S5-S6, where similar trends are observed, with intervention strategies
279 generally promoting volume growth compared with mice that did not receive an intervention.
280

281 **Intervention effects on memory performance**

282

283 After the final MRI scan, mice underwent the novel object recognition (NOR) and Morris water
284 maze (MWM) tests (see Materials and Methods, 'Behavioural tests') to assess recognition and
285 spatial memory differences between groups. In the NOR test, mice were exposed to familiar and
286 novel objects. Because mice prefer novelty, if the mouse remembers the familiar object, it will
287 spend more time exploring the novel object (Lueptow, 2017). This paradigm assesses short-term
288 recognition memory, which relies on the perirhinal cortex and dorsal hippocampus (Antunes and
289 Biala, 2012). In contrast, the MWM assesses long-term spatial memory dependent on the
290 hippocampus (Bromley-Brits et al., 2011). In the test, mice are trained to find a hidden escape
291 platform in a water-filled tank and are expected to remember the platform's location based on

292 spatial cues in the room during the probe trial (Bromley-Brits et al., 2011). Variables of interest
293 for the NOR included the percentage of time spent near the novel object and the discrimination
294 index (Antunes and Biala, 2012), which quantifies preference for the novel object. It is calculated
295 as the difference in time spent exploring the boundary of the novel versus familiar objects, divided
296 by total exploration time, with higher values indicating better recognition memory. For the MWM,
297 Gallagher's cumulative measure (GCM) (Pereira and Burwell, 2015) and the number of pass-
298 throughs were analyzed. Lower GCM values reflect more efficient learning, while higher counts
299 of passages near the location where the platform was previously located (pass-throughs) indicate
300 better spatial memory (Maei et al., 2009). These outcomes represent standard measures commonly
301 reported in the literature. Under standard chow conditions, MWM deficits typically emerge around
302 6 months (Billings et al., 2005; Webster et al., 2014), with NOR impairments appearing near 9
303 months (Clinton et al., 2007; Webster et al., 2014). Although exposure to a high-fat diet can shift
304 and accelerate this trajectory (Kim et al., 2017; Knight et al., 2014; Sah et al., 2017), reported
305 outcomes remain inconsistent due to variations in feeding duration and experimental windows.
306 Behavioural outcomes were analyzed using regression models appropriate for each variable, with
307 sex and genotype included as modeled factors. For each outcome, competing models with and
308 without higher-order interactions were compared to determine the most appropriate representation
309 of the data (for NOR: *Behavioural Outcome ~ Intervention * Genotype * Sex* or *Behavioural*
310 *Outcome ~ Intervention * Genotype + Sex*. For MWM: *Behavioural Outcome ~ Intervention **
311 *Genotype * Sex + Software + Weight* or *Behavioural Outcome ~ Intervention * Genotype + Sex +*
312 *Software + Weight*). For details, see Statistical Analyses, section 'Weight and behaviour'. As a
313 result, intervention effects are reported as model-based marginal contrasts, which estimate the
314 direction and magnitude of expected change in each behavioural outcome under a given

intervention, relative to Control, while adjusting for the covariates in the selected model. Confidence intervals that include zero indicate that the estimated intervention effect is not statistically different from the Control.

In the NOR test, WT males in the Exercise intervention showed reduced exploration time ($p = 0.02$) and increased immobility ($p = 0.01$), whereas WT females receiving the combined intervention travelled less ($p = 0.009$) and spent more time immobile ($p = 0.02$). These patterns suggest altered activity or anxiety-like behavior rather than global memory deficits (Supplementary Table S1).

In the MWM, a high-fat diet alone did not impair spatial memory at six months, as reflected by GCM and pass-throughs (Fig. 6A-B). In contrast, interventions improved performance in several sex- and genotype-specific combinations. WT males in the combined intervention and WT females in the Diet intervention showed reduced GCM ($p < 0.05$), indicating more efficient learning. Males from both genotypes in the combined intervention also exhibited increased pass-throughs ($p < 0.01$), consistent with improved spatial memory. Female mice displayed more selective effects, including increased pass-throughs in WT Exercise ($p = 0.04$) and reduced performance in 3xTgAD females under the Diet intervention ($p = 0.003$) (Fig. 6A-B).

Quadrant occupancy further highlighted sex- and genotype-specific effects (Fig. 6C). WT males in the combined intervention spent 19.5% more time in the target quadrant (the location of the platform during training), indicating improved performance ($p = 0.007$), whereas WT males on a high-fat diet spent 17.7% less time in this quadrant ($p = 0.009$), reflecting poorer performance. In 3xTgAD females, the combined intervention and Diet reduced time in the target quadrant by 20.0% and 14.0%, respectively ($p < 0.05$), while 3xTgAD males in the combined intervention showed a 19.0% increase (improved performance) ($p = 0.047$).

Together, these findings suggest that a high-fat diet did not produce widespread memory deficits at this age, but that interventions can modulate memory-related outcomes in a sex- and genotype-dependent manner, with males generally benefiting from the combined intervention.

Multivariate analyses of neuroanatomical changes, interventions, and behaviour

Given the high dimensionality of our data, which include 10 groups, thousands of voxels, and over 30 behavioural variables, we used Partial Least Squares (PLS) analysis, a multivariate method that identifies relationships explaining shared variance across datasets (Rännar et al., 1994). In this study, we applied behavioural PLS, in which brain measurements (voxel-wise log-Jacobian values) and behavioural variables (derived from MWM and NOR tests, intervention assignment, and demographics) were used as inputs. This approach enables dimensionality reduction while preserving the covariance structure of the data, allowing detection of patterns that may not be apparent when variables are examined individually. Mice in the combined intervention groups were excluded due to missing behavioural data (see Materials and Methods, 'Partial Least Squares analysis').

PLS treats each of the two input matrices, here behaviour and brain measurements, as "blocks" and iteratively transforms them to find the maximum overlap between the two (maximized shared variance) (Gerlach et al., 1979). For details on these transformations, refer to McIntosh and Misic, 2013 (McIntosh and Mišić, 2013). PLS produces several latent variables (LV), each of which encompasses a combination of one brain pattern and one behavioural pattern that maximally covary together and that explain a percentage of the covariance among the data. The LVs are

361 ordered according to the amount of covariance they explain, such that the first LV (LV1) captures
362 the largest overall shared variance between behaviour and brain measures. However, subsequent
363 LVs capture additional orthogonal patterns of covariation independent of earlier LVs and may
364 reflect relationships, including intervention-related effects, that are not dominant at the global
365 level. To determine whether each LV represented a statistically significant brain-behaviour
366 relationship rather than a chance association, significance was assessed using permutation testing
367 (3000 permutations), while standard errors and confidence intervals were estimated via bootstrap
368 resampling (3000 samples). Voxel-wise bootstrap ratios (BSRs) were then used to identify
369 significant brain regions contributing to each LV. BSRs were thresholded at ±1.96, corresponding
370 to a 95% confidence interval (see Statistical Analyses, section 'Partial Least Squares analysis').
371 While permutation-based inference is a standard approach, recent work from our laboratory
372 (Danyluik et al., 2024) recommends that the significance of LVs be evaluated using measures
373 beyond permutation-based p-values. In line with those findings and field standards (McIntosh and
374 Lobaugh, 2004), we interpreted the LVs based on the convergence of three factors: statistical
375 significance, the amount of covariance explained (LV strength), and the reliability of its spatial
376 patterns across bootstrap resampling. This approach ensures that our reported results reflect robust
377 patterns rather than artifacts of the permutation procedure.
378 A total of 45 latent variables (LVs) were obtained, corresponding to the number of behavioural
379 measures analyzed. Permutation testing identified four significant LVs (LV1–LV4; $p = 0.0170$,
380 0.0010, 0.0010, and 0.0013), which explained 29.36%, 13.44%, 12.46%, and 7.68% of the total
381 covariance, respectively. The significance and covariance explained by all 45 LVs are shown in
382 Supplementary Fig S8.

383 LV1 explained 29.36% of the covariance (Supplementary Fig S9A). It was characterized by
384 positive brain loadings (positive BSR) in the cerebellum, olfactory bulbs, and hippocampus. This
385 brain pattern was associated with wild-type mice, lower body weight, and better memory
386 performance, representing the healthiest mice with no AD-like characteristics.
387 LV2 accounted for 13.44% of the covariance (Supplementary Fig S9B) and displayed negative
388 loadings in the cerebellum and hippocampus, alongside widespread increases in the caudoputamen
389 and cortex. This pattern correlated with male 3xTgAD mice, higher body weight, and poorer
390 memory, reflecting mice at risk of developing AD-related features.
391 LV3 explained 12.46% of the covariance (Fig 6D-E) and was characterized by positive BSR in the
392 hippocampus and cerebellum. It correlated positively with low-fat diet and physical activity
393 interventions, negatively with no intervention and higher weight, and with better cognitive
394 performance on the MWM (GCM, pass-through, and time in the target quadrant). LV3 captured
395 intervention-related effects in a data-driven, anatomically unconstrained way, highlighting
396 widespread changes including the hippocampus and cerebellum, and aligned with patterns
397 observed in volumetric and voxel-wise analyses.
398 LV4 explained 7.68% of the covariance (Supplementary Fig S9C) and displayed negative and
399 positive BSRs across multiple regions, including positive loadings in the olfactory bulbs. This LV
400 was associated with wild-type mice.
401 Given that LV3 was the only LV capturing a correlation between brain volume changes and
402 intervention strategies, we examined brain scores, which reflect how strongly each mouse
403 expresses the brain pattern of an LV. Corresponding behaviour scores indicate how well each
404 mouse exhibits the behavioural pattern of the LV. Brain scores for LV3 were plotted against body
405 weight, GCM, and number of pass-throughs.

406 A negative correlation with weight (r = -0.35; Supplementary Fig S10) indicated that heavier mice
407 were less likely to exhibit the LV3 brain pattern, suggesting an inverse relationship between
408 cerebellar and hippocampal volumes and body weight. Brain scores also negatively correlated with
409 GCM (r = -0.27; Supplementary Fig S11A), consistent with better spatial memory performance,
410 and positively correlated with pass-through counts (r = 0.42; Supplementary Fig S11B), indicating
411 improved learning and memory of the platform's location.
412 Lastly, we plotted brain scores per group (Fig 6F) and found higher brain scores for groups that
413 received diet and exercise interventions, meaning the brain pattern of LV3 was better representing
414 mice in the physical activity and low-fat diet groups. Plots of group-wise brain scores for other
415 LVs support that LV1 is better at representing WT mice (Supplementary Fig S12A), LV2 is better
416 at representing 3xTgAD mice, with a higher brain score median for 3xTgAD mice that didn't
417 receive any intervention (Tg_HighFat, Supplementary Fig S12B), and LV4 is capturing features
418 of WT mice (Supplementary Fig S12C).
419

420 **Biological processes underlying the anatomical signature of LV3**

421

422 Given that the LV3 brain pattern was associated with intervention strategies, we hypothesized that
423 these interventions contributed to the observed structural pattern. This hypothesis is grounded in
424 prior evidence that these interventions influence neuroanatomy (Brown et al., 2022; Jensen et al.,
425 2021; Raji et al., 2024) and metabolic pathways (Gondim et al., 2015; Macedo et al., 2020).
426 Under this assumption, we examined the biological processes potentially driving LV3 by
427 comparing its spatial brain pattern with gene expression data from the Allen Mouse Brain Atlas
428 (Arnatkevičiūtė et al., 2019; Lein et al., 2007; Wang et al., 2020). Genes were ranked by Spearman

429 correlation, followed by a spatial gene enrichment analysis (SGEA) to statistically identify
430 overrepresented biological processes (GO terms) (Reijnders and Waterhouse, 2021), whose gene
431 expression patterns resemble the LV3 spatial brain pattern. See Materials and Methods, section
432 'Spatial Gene Enrichment Analysis' for details.
433 Seven significant GO terms emerged (Fig 6G), highlighting key biological processes: 1) Negative
434 regulation of response to oxidative stress, a process that reduces, prevents, or stops responses to
435 oxidative stress (GO:1902883); 2) Glucose homeostasis, which refers to the maintenance of a
436 stable internal glucose level within an organism or cell (GO:0042593); 3) Carbohydrate
437 homeostasis: the regulation of stable carbohydrate levels within an organism (GO:0033500); 4)
438 Cellular glucose homeostasis: the maintenance of glucose levels specifically within a cell
439 (GO:0001678); 5-6) Cellular response to hexose/glucose stimulus: a process where cells alter their
440 state or activity in response to hexose/glucose (GO:0071331 and 0071333); and 7) Positive
441 regulation of fatty acid transport: a process that increases or activates the transport of fatty acids
442 (GO:2000193).
443 The ancestry analysis of cellular response to glucose stimulus (GO:0071333) (EMBL-EBI, n.d.)
444 revealed hierarchical relationships with carbohydrate homeostasis, glucose homeostasis, cellular
445 glucose homeostasis, and cellular response to hexose stimulus. This suggests a coordinated
446 regulatory network controlling glucose metabolism. In contrast, negative regulation of oxidative
447 stress response and positive regulation of fatty acid transport were independent, indicating distinct
448 pathways.
449

450 # Discussion

451

452 While there are no disease-modifying treatments for AD, reducing the incidence of new cases
453 through intervention strategies emerges as an important approach to addressing this global
454 challenge (Alwan et al., 2024). In this manuscript, we leveraged neuroimaging techniques to study
455 the effects of a high-fat diet on the mouse brain and how intervention strategies, including physical
456 activity, a low-fat diet, or their combination, can mitigate these effects. We collected a unique
457 dataset encompassing 156 mice, divided into similar groups per genotype (3xTgAD and WT),
458 balanced for sex. In these groups, we evaluated weight, behaviour, and neuroanatomy, and used
459 multivariate analysis to find hidden patterns in the data that led to the discovery of possible
460 biological processes behind the impact of exercise and a change to a low-fat diet. Although our
461 focus was not to understand how interventions delay or prevent dementia, our findings support
462 their role in promoting brain health by reversing the effects of a high-fat diet in mice.
463
464 To evaluate neuroanatomical changes, we used volumetric and DBM analyses. DBM provides
465 insights into subtle, region-specific deformations that volumetric measures may overlook. We
466 found that genotype itself affected the cortex volume, as found before in previous work done in
467 our lab (Kong et al., 2018; Rollins et al., 2019). In addition, we found pronounced changes in the
468 olfactory bulbs, hippocampus, caudoputamen, and cerebellum, which replicate work from our lab
469 aimed at characterizing the neuroanatomical trajectories of the 3xTgAD mice (Kong et al., 2018).
470 We also found that a high-fat diet affected the hippocampus and cerebellum (in WT mice only),
471 structures that have been shown to present modifications with a high-fat diet or obesity in both
472 rodents and humans, impacting neurogenesis and synaptic plasticity in the hippocampus in rodents
473 (González Olmo et al., 2023; Lindqvist et al., 2006), and causing decreased volume in the left
474 cerebellum in both adults and children (Herrmann et al., 2019; Ou et al., 2015). The lack of effects

475 of a high-fat diet on 3xTgAD mice could be attributed to their genetic predisposition, which is
476 linked to neuroanatomical vulnerabilities (Esquerda-Canals et al., 2013; Gama Sosa et al., 2010;
477 Kong et al., 2018). This genetic vulnerability could explain why we found smaller volumes for the
478 cerebellum and hippocampus in 3xTgAD mice.
479
480 Peak voxels allowed us to understand the effect of intervention strategies. In many instances, we
481 noticed that the interventions affected the voxel-wise volumes (either expansions or contractions)
482 to comparable levels as the control groups, even exceeding those levels for the groups that received
483 a combined intervention. In animal models, a high-fat diet increases microglial activation (Knight
484 et al., 2014), causes changes in hippocampal mitochondrial morphology, and leads to a reduction
485 in synapse number (Martins et al., 2017). On the contrary, voluntary physical activity has been
486 shown to increase dendritic complexity in the dentate gyrus (Redila and Christie, 2006), regulate
487 synaptic transmission in the hippocampus (Vaynman et al., 2006), promote angiogenesis after an
488 ischemic injury (Tang et al., 2018), and increase the volume of both hippocampus and cerebellar
489 regions (Cahill et al., 2015), while a low-fat diet has not been well studied in terms of effects at
490 the microscopic level. Of interest, a study evaluating the same interventions as in this work found
491 that they mitigate high-fat diet-related amyloid-β accumulation and memory impairments in
492 transgenic mice that overexpress the human amyloid-β precursor protein (APP) in the
493 hippocampus (Maesako et al., 2012).
494
495 We studied the 3xTgAD mice to model AD-relevant susceptibility to risk factors. These mice have
496 transgenes for APPSWE and PS1M146V, along with an extra mutation associated with
497 frontotemporal dementia, tauP301L, resulting in the formation of both Aβ plaques and

498 neurofibrillary tangles in the model (Oddo et al., 2003). Previous studies indicate that, by 6 months
499 of age, these mice exhibit early hippocampal pathology, with some amyloid-β accumulation and
500 tau phosphorylation (Belfiore et al., 2019; Jullienne et al., 2022). Importantly, in line with prior
501 literature, spatial memory deficits assessed by the MWM can appear as early as 6 months, whereas
502 recognition memory impairments assessed by the NOR test tend to emerge later, around 9 months
503 (Webster et al., 2014). Consistent with these expectations, we observed behavioural effects in the
504 MWM at 6 months, whereas NOR performance remained largely unaffected. Notably, these effects
505 were selective for genotype and sex. These behavioural and neuroanatomical findings suggest that
506 young adult mice, particularly 3xTgAD mice, may exhibit resilience to the high-fat diet, limiting
507 the manifestation of deficits. Notably, 3xTgAD mice already show smaller brain volumes at
508 baseline, which may constrain the detectable impact of the diet. Nevertheless, interventions such
509 as exercise appear to support brain structure and function even in the absence of pronounced high-
510 fat diet impairments, potentially by enhancing compensatory or protective mechanisms.
511
512 In this work, sex was included as a biological variable in all statistical models. Overall, sex-related
513 effects were most apparent for body weight and behaviour. Males in the combined diet and exercise
514 group showed weight loss, whereas females generally exhibited weight stabilization. Behavioural
515 outcomes also differed by sex, with improvements in spatial memory being more consistently
516 observed in males, while females showed more variable responses depending on genotype and
517 intervention. By contrast, neuroanatomical measures were less sensitive to sex, as neither region-
518 based volumetry nor voxel-wise DBM revealed significant sex differences after correction for
519 multiple comparisons. Together, these findings indicate that, within the age range examined, sex

contributes to differences in some of the responses to interventions, whereas structural brain changes appear largely similar between males and females.

Using a multivariate approach (PLS), we identified a brain pattern characterized by positive loadings in the cerebellum and hippocampus, which negatively correlated with a high-fat diet and positively correlated with physical activity and diet interventions. Importantly, this pattern was delineated without relying on predefined neuroanatomical boundaries, demonstrating the power of data-driven methods to capture complex interdependencies across thousands of voxels. Nevertheless, the interpretation of patterns derived from dimensionality reduction approaches remains an active area of discussion (Danyluik et al., 2024; Liu et al., 2022; Tang et al., 2022). Work from our laboratory (Danyluik et al., 2024) suggests that the primary latent variable can often appear significant due to the inherent permissiveness of the Procrustes-rotated permutation test. To ensure the patterns reported here are robust for interpretation rather than a statistical artifact, we integrated the significance along with the latent variables' strength and their spatial stability through bootstrapping, as evidenced by the high voxel-wise bootstrap ratios in the cerebellum and hippocampus. The convergence of these metrics suggests that the patterns found here encode meaningful neurobiological features that may help us find the underlying biological mechanisms, as exposed by our further SGEA analysis.

Previous work correlating spatial neuroanatomical changes to spatial patterns of gene expression data found that changes in neuroanatomy can help pinpoint genes responsible for the observed phenotypes (Fernandes et al., 2017). Here, the SGEA analysis correlating gene expression data to the PLS-LV3 brain pattern uncovers GO terms associated with biological processes such as

543 glucose homeostasis and positive regulation of fatty acid transport. Here, five out of the seven
544 significant terms are related to glucose homeostasis. These processes have been discovered
545 through other studies, for example, a study in a transgenic model for AD (and WT counterpart)
546 found that a low-fat diet reversed the alterations in glucose metabolism in mice fed a high-fat diet,
547 taking glucose to comparable levels as control mice (fed with a low-fat diet) (Walker et al., 2017).
548 Another study found that a high-fat diet enhanced glucose intolerance in a transgenic model of
549 AD, reversible with the injection of insulin (Vandal et al., 2014). We also found an association
550 with a negative regulation of the response to oxidative stress. In work from Sah et al., a high-fat
551 diet exacerbated oxidative stress in 3xTg-AD mice by inactivating Akt-Nrf2 signaling and
552 reducing downstream antioxidant enzymes, leading to neuronal apoptosis and early cognitive
553 decline (Sah et al., 2017). Lastly, it has been reported that exercise could promote regulation of
554 oxidative stress and regulation of fatty acid transport (Camiletti-Moirón et al., 2013; Liśkiewicz et
555 al., 2020; Souza et al., 2022). For example, a study found that exercise decreased reactive oxygen
556 species in rats fed with a high-fat diet (Molteni et al., 2004).
557
558 The data we gathered indicates a potential function of the cerebellum that merits further
559 investigation. Traditionally, the cerebellum has been associated with motor control; however, new
560 evidence supports that it might also be related to cognitive functions (Koziol et al., 2014). Previous
561 research shows a decrease in the neuronal density in both the cerebellar cortex and deep nuclei of
562 the cerebellum in 3xTgAD mice (Esquerda-Canals et al., 2013). This suggests a genetic
563 vulnerability in 3xTgAD mice, which may contribute to the pronounced cerebellar changes
564 observed. Another study found that APP and apoptosis-related molecules (e.g., caspases) increase
565 in the cerebellum of WT mice after only 7 days on a high-fat diet (Xu et al., 2021). A study on

566 children found that physical fitness was associated with larger volumes in some regions of the
567 cerebellum (Jalanko et al., 2024). Another study showed that children who reported difficulty
568 controlling how much they eat had lower grey matter in the parahippocampal gyrus and the left
569 cerebellar lobule VI (Pearce et al., 2023). It has been proposed that since eating behaviours are
570 influenced by predictions (e.g., hunger before a meal, or expectations of food taste) and feedback
571 (e.g., satiety after eating), the cerebellum might be involved in managing prediction errors in these
572 domains, adjusting responses to align with sensory feedback and expectations across motor,
573 cognitive, and affective processes (Iosif et al., 2023).
574
575 In terms of limitations, our study used a high-fat diet in which 60% of calories were derived from
576 fat. While high-fat diets for mice typically range between 40–60% of calories from fat, with
577 varying compositions of saturated and unsaturated fatty acids (Lai et al., 2014), this level
578 substantially exceeds the fat intake commonly observed in humans. For example, in the U.S., fat
579 accounts for approximately 30-40% of total calories (Ford and Dietz, 2013), and the most recent
580 report from Canada (2000) indicates a similar intake of around 30% (Gray-Donald et al., 2000).
581 Consequently, the effects observed in our animal model may not fully reflect human dietary
582 patterns. Another limitation is that we used young adult mice (up to 6 months old), corresponding
583 to early adulthood in humans (Cottam et al., 2025). This restricts the generalizability of our
584 findings, as resilience and susceptibility to interventions may change with age. Nevertheless,
585 studying early-life exposures in preclinical models remains valuable, as it can provide insights into
586 mechanisms and potential intervention strategies during the extended preclinical phase of
587 dementia. Additionally, our findings related to the biological processes behind interventions
588 should be confirmed. Future work should address this question as well as the best timing for the

589 initiation of these interventions. Finally, we acknowledge that the use of non-littermate WT
590 controls may introduce confounds such as gut microbiome heterogeneity (McCoy et al., 2017).
591 However, because the primary aim of this study was to evaluate the effects of a high-fat diet and
592 subsequent interventions, we utilized intra-genotype comparisons. This approach reduces the
593 influence of baseline differences between WT and 3xTgAD on the interpretation of treatment
594 effects; however, such baseline variability should be considered when interpreting genotype
595 effects (comparisons between WT_Control and Tg_Control).
596 In summary, our findings underscore the potential of diet and exercise interventions to counteract
597 the adverse effects of a high-fat diet on the brain, particularly in the cerebellum and hippocampus.
598 Additionally, they highlight the necessity for more research to investigate the underlying
599 mechanisms and the applicability of these findings to human health.
600

601 # Materials and Methods

602

603 ### Animals

604

605 All animal experiments were carried out following the Canadian Council on Animal Care and
606 approved by the McGill University Animal Care Committee (Montreal, QC, Canada). Male and
607 female homozygous 3xTgAD mice (https://www.jax.org/strain/004807, RRID:
608 MMRRC_034830-JAX) and non-transgenic Wild-Type (WT) B6129SF2J mice
609 (https://www.jax.org/strain/101045, RRID: IMSR_JAX:101045) were acquired through the
610 Mutant Mouse Resource and Research Center (MMRRC) and were bred on an F2 hybrid cross
611 between C57BL/6J females (B6) and 129S1/SvImJ males (129S). The 3xTgAD mice have a

612 knocked-in PS1M146V mutation at the mouse PSI locus and two human transgenes: APPSwe and
613 tauP301L (Oddo et al., 2003). The PS1M146V and APPSwe mutations affect the processing of
614 the amyloid-beta precursor protein (APP) into Amyloid-beta (Duff et al., 1996), while TauP301L
615 induces tauopathy (Lewis et al., 2000). It has been reported that 3xTgAD exhibits cognitive
616 impairments related to memory retention at four months of age, accumulating intraneuronal
617 amyloid plaques in the cortex, hippocampus, and amygdala (Billings et al., 2005). Other studies
618 have reported cognitive impairment, amyloid plaques, and neurofibrillary tangles in the
619 hippocampus at six months of age (Belfiore et al., 2019). A recent characterization of 3xTgAD
620 mice reported a shift in timing in plaque and tangles appearance, with a substantial impact on
621 females due to estrogen-regulated gene promoters (Javonillo et al., 2022; Sadleir et al., 2015).
622 Mice were bred in an in-house colony, and their offspring were weaned during the fourth week
623 after birth. The offspring were housed in groups of three to four mice per cage at the Douglas
624 Mental Health University Institute's Animal Facility (Montreal, QC, Canada) in standard housing
625 conditions (12h light/dark cycle, with lights on at 8:00 am). Mice received ad libitum access to
626 food and water at all times.
627

628 ## Experimental design

629

630 All mice were on a standard diet from weaning until two months of age (2016 Teklad Global 16%
631 Protein Rodent Diet, Inotiv, Madison, Wisconsin, USA), containing 4% fat from soybean oil,
632 formulated for growth and maintenance. At two months, 80% of both 3xTgAD and WT mice were
633 randomly assigned to an obesity-inducing high-fat diet (Teklad high-fat diet TD.06414 with 60%
634 of kcal from fat, primarily lard, Inotiv, Madison, Wisconsin, USA), while the remaining mice were

635 transitioned from standard diet to the low-fat control diet (Teklad Purified Control Diet TD.08806
636 with 10.5% of kcal from fat, primarily soybean oil and lard, Inotiv, Madison, Wisconsin, USA).
637 The control diet is formulated by the manufacturer as the appropriate ingredient-matched control
638 for the high-fat diet, differing only in its macronutrient composition but matched for ingredients
639 and processing. This approach helps isolate the effects of fat content, minimizing confounding
640 variables related to food composition or manufacturer. For four to six months, mice fed a low-fat
641 diet continued on it and served as controls (groups: WT_Control and Tg_Control), while a subset
642 of mice on the high-fat diet remained on it (WT_Highfat and Tg_Highfat). During this same period
643 (4-6 months), to assess the reversibility of the induced obesity, the rest of the mice fed with the
644 high-fat diet were randomly assigned to either a low-fat diet intervention (groups: WT_Diet and
645 Tg_Diet), physical activity while still on the high-fat diet (groups: WT_Exercise and Tg_Exercise)
646 or the combination of exercise and a low-fat diet (groups: WT_Both and Tg_Both). In the physical
647 activity groups, mice had access to a running wheel for voluntary physical activity. Food intake
648 was not monitored due to the difficulties in obtaining accurate measurements as a result of
649 communal housing (Starr and Saito, 2012). Similarly, mice were not placed in isolation to
650 accurately measure wheel use because this introduces the effect of social isolation, which is also a
651 risk factor for AD (Goh and Ladiges, 2015; Huang et al., 2015; Ren et al., 2023). Weight
652 measurements were collected for at least 18 weeks, from two to six months of age (N = 156 mice
653 with 18 measurements each). T1-weighted MRI scans were acquired at two, four, and six months,
654 followed by behavioural testing with the MWM and NOR tests at six months of age. Out of the
655 initial 165 mice involved (around 16 mice per group and a nearly equal number of males and
656 females), 9 died or were sacrificed before the final neuroimaging timepoint, primarily due to fatal
657 injuries as a result of fighting (four males and one female) which was precipitated primarily by the

658 introduction of the running wheel (fighting caused an entire cage of 3xTgAD mice in the combined
659 intervention to be sacrificed), but also from hydrocephalus (one male, one female), and
660 complications as a result of $MnCl_2$ injections (which were needed for improve MRI contrast) (two
661 males). Fig 1A shows the experimental workflow, Supplementary Table S3 describes the nutrient
662 information per diet, and Supplementary Table S4 shows the timeline at which each group received
663 their respective diets and the N per group at each scanning time point.
664

665 ## Magnetic Resonance Image acquisition

666

667 T1w MRI images were acquired at three time points, when mice were two, four, and six months
668 old. These time points were selected to capture the neuroanatomy at baseline, before, and after
669 interventions. Scans were collected using a 7T small animal scanner (Bruker Biospec 70/30 USR;
670 30-cm inner bore diameter) at the Douglas Mental Health University Institute (Montreal, QC, CA).
671 Mice were injected 24 hours before the scanning with a bicine-buffered solution of manganese (II)
672 chloride ($MnCl_2$) titrated with 1M sodium hydroxide (NaOH; Sigma Aldrich, Switzerland) at a
673 dosage of 62.5 mg/kg. $MnCl_2$ enhances the contrast of T1w structural MRI scans due to the
674 paramagnetism of Mn_{2+} that reduces the T1 relaxation time, enhancing the contrast between tissues
675 (Lee et al., 2005; Yang and Li, 2020). NaOH and bicine were added to mitigate the acidic
676 environment caused by $MnCl_2$, preventing tissue damage at the injection site and keeping the pH
677 at about 7.4 (Seo et al., 2011). Dosage was calculated based on weight at baseline to avoid toxic
678 doses in obese mice. High doses were observed to cause skin lesions in previous work from our
679 group (Rollins et al., 2019). The injection was administered to the intraperitoneal cavity to limit
680 toxicity (Kuo et al., 2005). Before the scanning, animals were anesthetized with isoflurane

681 (Fresenius Kabi Canada Ltd, Richmond Hill, CA) at 5% and injected with 0.5 mL of 0.9% sterile
682 sodium chloride physiological solution (Sigma Aldrich). During the scanning, mice were
683 maintained under 1-2% isoflurane, with breathing rate monitored and maintained at 30-100 breaths
684 per minute. The sequence used to acquire the images was a 3-dimensional fast low-angle shot (3D
685 FLASH), and the final T1w MRI was generated from an average of two acquisitions (TR = 20 ms,
686 TE = 4.5 ms, matrix size = 180 x 160 x 90, voxel dimensions = 100 μm isotropic, and flip angle =
687 20°) and fat suppression. Images were collected with the Bruker 23 mm volumetric
688 transmit/receive quadrature coil (Anastassiadis, 2020).
689

690 ## Image processing

691

692 Raw Digital Imaging and Communications in Medicine (DICOM) scans were converted to the
693 Medical Imaging Net CDF (MINC) file format and preprocessed with a set of tools and libraries
694 developed in our laboratory and at the Montreal Neurological Institute (MNI), freely available
695 online (Minc-toolkit 1.9.16, RRID: SCR_014138). Preprocessing included stripping images of
696 their native coordinate system, left-right flipping of images to compensate for the scanner's native
697 radiological coordinate system, denoising using a patch-based non-local means filter previously
698 validated (Coupe et al., 2008), and affine registration to an average mouse template to produce a
699 brain mask. N4ITK was used as an improved version of the N3 bias field correction algorithm for
700 inhomogeneity correction at a minimum distance of 5 mm (Tustison et al., 2010). Then, a de-
701 scaled and de-sheared version of the affine registration was used to perform a rigid alignment of
702 the scan to the mouse template space (Gallino et al., 2019). Images were inspected using the
703 Display visualization software of MINC tools. Quality control was performed for each time point.

704 The inspection was mostly focused on detecting the presence of hydrocephalus or motion-related
705 artifacts. Of the 165 scans collected at timepoint one, 160 passed quality control
706 (https://github.com/CoBrALab/documentation/wiki/Mouse-QC-Manual-(Structural)); from the
707 160 scans collected at timepoint two, 148 passed; and from the 156 scans collected at timepoint
708 three, 145 passed quality control. Therefore, we used 453 brain images for further analysis.
709

710 ## Volumetric analysis

711

712 We performed a volumetric analysis on mice with at least one image that passed quality control
713 (total N = 161 mice, 453 scans) to study whether the high-fat diet and intervention strategies
714 impacted the neuroanatomy of 3xTgAD and wild-type mice. We parcellated the brain into 182
715 structures per hemisphere according to the DSURQE (Dorr-Steadman-Ullmann-Richards-Qiu-
716 Egan) mouse brain atlas (Dorr et al., 2008; Richards et al., 2011; Steadman et al., 2014; Ullmann
717 et al., 2013) using the Multiple Automatically Generated Templates (MAGeT) brain segmentation
718 algorithm (Chakravarty et al., 2013). MAGeT first performs a non-linear transformation between
719 the input data (T1w MRI scans) and the input atlas. The atlas is registered to a small subset of the
720 subject images (n=21). These labeled images are used as a template library, and pairwise non-
721 linear transformation is performed to generate as many segmentations per subject as there are
722 templates in the library (n=21). Given there are now 21 'atlases', these brains are now registered
723 to each subject such that the final segmentation is produced by a voting procedure at the voxel
724 level, where the most voted label is selected. Quality control of the outputs was performed by
725 visually inspecting each segmentation overlaid on each mouse scan and verifying that the labels
726 matched the brain anatomy (https://github.com/CoBrALab/documentation/wiki/MAGeT-Brain-

727 Quality-Control-(QC)-Guide). Out of 453 MAGeT segmentations, 385 passed quality control,
728 corresponding to scans from 157 mice: 139 scans from the first timepoint, 116 scans from the
729 second, and 130 scans from the third. Due to frequent artifacts in the olfactory bulbs, labels from
730 this region were excluded from the volumetric analysis (see Supplementary Table S5).
731 Importantly, these artifacts did not impact the voxel-wise analysis detailed in the following section.
732 Volumes were computed from these segmentations based on the number of voxels labelled for
733 each region and the voxel dimensions.
734

735 ## Deformation-based morphometry analysis

736

737 After the volumetric study, we aimed to analyze the changes in volume without any *a priori*
738 assumptions on neuroanatomical boundaries. We applied a deformation-based analysis pipeline to
739 model voxel-wise volume changes using the Jacobian determinant, which measures voxel
740 contraction or expansion relative to a template (Chung et al., 2001; Lau et al., 2008). Images from
741 mice with at least two time points that passed quality control (N = 152 mice, 423 images) served
742 as input. To study overall brain differences, absolute Jacobians modeling the linear and non-linear
743 transformations were generated using the two-level model-building toolkit Pydpiper (Friedel et al.,
744 2014). Images were non-linearly registered to create a population-specific average template,
745 followed by a group-wise registration to account for the longitudinal nature of our data (Friedel et
746 al., 2014). The non-linear registration was performed using the diffeomorphic MINC Advanced
747 Normalization Tools (mincANTs) algorithm (Avants et al., 2011, 2009). The absolute Jacobians
748 were log-transformed and blurred (0.2 mm full-width at half-maximum) to conform to Gaussian
749 assumptions for statistical testing (Chung et al., 2001; Gallino et al., 2019). For within-subject

750 registration, an average representation of each specific subject's anatomy over time was created
751 using a hierarchical multi-resolution registration strategy (Avants et al., 2009). These subject-
752 specific averages served as inputs to build the group average and the common space for group-
753 wise and longitudinal comparisons (Gallino et al., 2019; Kong et al., 2018). Resampled absolute
754 Jacobians adjusted for whole-brain size were used for all analyses. Jacobian determinants quantify
755 local volumetric differences relative to the population average, such that values greater than 1
756 indicate local expansion (relative to the population reference) and values less than 1 indicate local
757 contraction; values equal to 1 indicate no change. For voxel-wise longitudinal examination of
758 volume over time between groups, a group-specific baseline mean was calculated for each group,
759 such that changes could be interpreted as deviations from baseline over time. These baseline-
760 centered values were subsequently exponentiated and expressed as volume percentage change
761 from baseline for improved visualization and interpretation.
762

763 **Partial Least Squares analysis**

764 To study the relationship between voxel-wise neuroanatomical changes and behavioural data, we
765 ran a behaviour Partial Least Squares analysis (PLS) in Matlab 2022a (PLScmd software;
766 Baycrest, Canada) as previously done in other work from our group (Guma et al., 2021). PLS can
767 be used when the number of features (e.g., voxel-wise data) is higher than the number of
768 observations (e.g., number of mice), despite the presence of correlated variables (collinearity)
769 (Cramer, 1993). We constructed a matrix (X) made of voxel-wise Jacobian values from the last
770 MRI scan collected (third timepoint, N = 96 mice). Another matrix (Y) was built with data from
771 45 variables, including demographics and behavioural data from the MWM and NOR tests. The

772 matrices X and Y were correlated and subjected to a mathematical process (singular value
773 decomposition) to obtain latent variables (LV). Only mice with complete MRI and behavioural
774 data were included; this led to the exclusion of mice in the groups that received the combined
775 intervention (Tg_Both and WT_Both). PLS produces as many LVs as there are variables in the
776 behavioural data, in our case, 45. LVs capture the maximal shared variation between the two data
777 sets, summarizing their relationship in a single dimension, and can be interpreted as maximally
778 covarying brain patterns and their associated behavioural factors (McIntosh et al., 1996).
779 Behavioural variables used for partial least squares analysis were: 1) Demographic**:** sex, genotype,
780 low-fat or high-fat diet, intervention type, no intervention; 2) Variables from Morris Water Maze:
781 total path in meters, total time, time in quadrant of interest, time and distance in other quadrants,
782 speed, count of passthroughs above the platform, passthroughs near the platform zone, GCM,
783 cumulative time in the platform zone; 3) Variables from the novel object recognition test: time in
784 the boundary of the novel object (seconds), time in the boundary of the familiar object (seconds),
785 percentage of time of exploration of the novel object, preference for novelty, frequency in the
786 novel object exploration, percentage of time of exploration in the boundary of the novel object,
787 percentage of time of exploration in the boundary of the familiar object, distance (meters), velocity,
788 frequency entering the arena, time spent in the arena (seconds), frequency entering the zone of the
789 novel object, frequency entering the zone of the familiar object, time spent in the zone of the novel
790 object (seconds), time spent in the zone of the familiar object (seconds), frequency entering the
791 zone of the boundary of the novel object, frequency entering the zone of the boundary of the
792 familiar object, time spent in the zone of the boundary of the novel object, time spent in the zone
793 of the boundary of the familiar object, frequency of high-mobility, cumulative time of high-

794 mobility, frequency in mobility, cumulative time of mobility, frequency in immobility, cumulative
795 time immobile, moving time, not moving time.
796

797 ## Spatial Gene Enrichment analysis

798 To assess the biological mechanisms underlying the brain pattern identified using PLS (latent
799 variable 3), we conducted a Spatial Gene Enrichment Analysis (SGEA) in R/4.1.3. We utilized
800 gene expression data from the Allen Institute's Mouse Brain Atlas (Lein et al., 2007), which
801 contains 4345 three-dimensional images of gene expression for 4082 unique genes acquired by
802 immunohistochemistry on brain slices from adult (P56) male C57Bl/6 mice. Additionally, we used
803 the high-resolution Allen Mouse Brain Common Coordinate Framework template (CCFv3, 200
804 μm voxel size) (Wang et al., 2020) to provide a standardized anatomical reference space, allowing
805 gene expression maps to be aligned and compared consistently across the brain. Gene annotations,
806 which link individual genes to specific biological processes (also called modules), were drawn
807 from the Gene Ontology (GO) consortium. We used the gene annotation dataset
808 MOUSE_GO_bp_no_GO_iea_symbol, with 15757 gene sets (Gene Ontology Consortium, 2015).
809 These annotations allow us to group genes into functional modules, providing biological context
810 for interpreting patterns of spatial gene expression. The annotations used here were inferred from
811 electronic evidence, meaning they were computationally predicted rather than manually curated.
812 The gene expression images and CCFv3 template were realigned to RAS+ orientation and
813 converted to the MINC format. Next, we conducted the SGEA analysis in R/4.1.3 using the
814 bootstrap ratio map from PLS latent variable 3 (LV3) as input. The map was thresholded at the
815 bootstrap ratio value of 1.95 (95% confidence interval) to include only regions contributing
816 significantly to LV3, and are therefore meaningfully related to behavioural measures. To explore

817 the molecular mechanisms underlying these patterns, the thresholded brain loading map was
818 spatially correlated with gene expression profiles. Genes were then ranked based on the strength
819 of their correlation with the brain pattern using Spearman correlation.
820

821 **Behavioural tests**

822

823 Novel Object Recognition (NOR) was performed one week after the third MRI scan, and the
824 Morris water maze (MWM) test was performed two days after the NOR test. For the NOR test, on
825 day zero, mice were placed in a cubic open field box (45 cm^3) with bedding from their cage. Mice
826 were allowed to explore for 10 min. On day one, mice were placed in the same box with bedding
827 from their home cage, and they were allowed to explore two identical objects (4 cm^3 each) for 10
828 min. The objects were spaced 20 cm apart. Mice were returned to their home cage, and one hour
829 later, they returned to the test box with one object replaced with the novel object. Mice were given
830 10 minutes to explore. The location of the novel object was randomized (left or right side) and
831 balanced across trials. The tests were conducted under a red light with an overhead camera. The
832 camera recorded the test, and the resultant video clips were converted from DAV to AVI and
833 further edited to last precisely 10 minutes. Videos were analyzed with Ethovision XT 12 Software.
834 Only data from the test trial was used. During analysis, a boundary area around the object was set
835 to 10 cm^2. To determine if mice spent more time around the novel object, the percentage of
836 exploration in the boundary zone of the novel object was calculated. To do so, the time spent in
837 the boundary area of the novel object was divided by the sum of the time spent in the boundary
838 area of the novel and the familiar object and multiplied by 100. Another variable of interest was
839 the discrimination index, also known as the discrimination ratio (Antunes and Biala, 2012). If

840 positive, the discrimination ratio indicates more time spent exploring the novel object. A value of
841 zero means equal time spent on both objects. This variable was calculated as the amount of time
842 spent exploring the boundary zone of the novel object minus the amount of time spent exploring
843 the boundary zone of the familiar object, divided by the total amount of time spent exploring the
844 boundary zone of both objects.
845 The MWM test was performed in a circular tank (120 cm in diameter) with water at 21-22 °C.
846 Water was made opaque by adding white, non-toxic tempera paint. There were three visual cues
847 on the interior wall of the tank above the water line (in the north, east, and southwest). An escape
848 platform with a diameter of 15 cm was used. On day zero, mice were habituated with a trial where
849 the escape platform was visible (1 cm above the water line). The anterior allowed the identification
850 of apparent sensorimotor deficits. From day one to five, mice were trained five times by entering
851 the tank with a non-visible escape platform always located in the southwest quadrant. During this
852 training, mice entered the tank from one of three starting points (northeast, southwest, and
853 southeast) in pseudorandom order. If the mice couldn't find the platform in 60 seconds, they were
854 gently guided towards it. A failure was a training in which mice didn't find the platform within 60
855 seconds. On day six (probe day), a single trial was performed. In this trial, the escape platform was
856 removed. Mice entered through the northeast point and were allowed 60 seconds to explore. Each
857 trial was recorded with a mounted camera above the tank. However, some mice were recorded
858 with a different camera due to software failure. Only data from the probe day was used. Mice were
859 excluded if they failed to find the platform in three of six training sessions. The data from the first
860 camera was analyzed with tracking software (HVS Image Ltd). The data captured with the second
861 camera was analyzed using a different software (Ethovision Noldus XT 12). Variables of interest
862 were further analyzed, such as the average cumulative distance from the platform (also known as

863 cumulative Gallagher's measure) and the number of pass-throughs (passages above the previous
864 platform location). The cumulative distance from the platform is recognized as a solid measure of
865 memory, and it has a good sensitivity to small differences in groups (Pereira and Burwell, 2015;
866 Vorhees and Williams, 2006).
867

868 # Statistical Analyses

869

870 ### Weight and behaviour

871

872 Body weight data were analyzed with Linear Mixed Effects (LME) models implemented in the
873 lme4 package in R (version 4.1.3). The model included a four-way interaction between time (in
874 weeks), intervention, genotype, and sex as fixed effects, with a random intercept and slope for
875 weeks at the individual level to account for repeated measurements within each mouse (*Weight* ~
876 *Week*Intervention*Genotype*Sex* + (*Week*|*ID*)).
877 Because higher-order interaction terms are difficult to interpret directly (Busenbark et al., 2022),
878 we estimated model-based rates of weight change over time using the 'marginaleffects' package
879 (version 0.28.0). These estimates (referred to as marginal comparisons) quantify the expected
880 change in body weight per week (g/week) for each combination of intervention, genotype, and sex.
881 Ninety-five percent confidence intervals (95% CI) were computed using the delta method as
882 implemented in 'marginaleffects' (Arel-Bundock, 2025).
883 Behavioural data derived from the MWM and NOR were statistically assessed using regression
884 models selected based on the properties of each variable. For each outcome, data distributions were
885 visually inspected using histograms (available in Supplementary Material, Fig S7) and formally

evaluated for normality within experimental groups using the Shapiro-Wilk test and for homogeneity of variance using Levene's test. No outliers were detected for MWM; however, three outliers were removed due to extreme values for NOR (One mouse from the WT_HighFat group and two mice from the Tg_HighFat group). Model families were chosen according to the outcome, for example, beta regression for bounded proportion outcomes, generalized linear models for count data, and hurdle models for zero-inflated outcomes. A detailed summary of these choices is available in Supplementary Material (Tables S1-2). For NOR, two competing models (*Behavioural Outcome ~ Intervention * Genotype * Sex* or *Behavioural Outcome ~ Intervention * Genotype + Sex*) were compared using model performance metrics within the 'model_performance' function from the 'performance' package (version 0.15.2) in R (version 4.4.3) to decide which model best fits the behavioural outcome being analyzed. For MWM, the same two competing models were compared, with additional covariates for *Software* (see Materials and Methods, section 'Behavioural tests' for more details) and *Weight* (*Behavioural Outcome ~ Intervention * Genotype * Sex + Software + Weight* or *Behavioural Outcome ~ Intervention * Genotype + Sex + Software + Weight*). To interpret significant interaction terms, model-based marginal contrasts were computed using the 'contrast' function from the 'marginaleffects' package. Marginal contrasts quantify the differences between each intervention and the Control (mice that remained on a low-fat diet throughout the experiment), while holding all other covariates at fixed values. These effects can be interpreted as the expected change in the outcome attributable to the intervention, independent of other variables in the model. Only mice with full behavioural data were included in the analyses. The number of mice per group for NOR and MWM is provided in Supplementary Table S6. Results were plotted using ggplot2 in R.

Volumetric and deformation-based analyses

The association between volume data derived from MAGeT and groups was evaluated with a hierarchical LME model with the RMINC/v1.5.3.0 package for R (Lerch et al., 2017). The model included volume per region as the dependent variable, an interaction between group and age in days, sex as an independent variable, and a random intercept allowed per mouse (*Volume* ~ *Group**poly(*Age*,2) + *Sex* + (*1*|*ID*)). The poly(*Age*,2) term allows the model to capture quadratic (second-degree polynomial) relationships between Age in days and volume while considering interaction effects with each group; data from the three time points were included. The linear mixed effects model output was corrected for multiple comparisons with False Discovery Rate (FDR) with a 10% threshold (Benjamini and Yekutieli, 2001), meaning that among the regions shown as significant, we expect at most 10% to be false positives. Results were plotted by overlaying the statistics map on top of the population average using functions available in RMINC. The plots display the linear terms of the interaction between group and age in days (*Group**poly(*Age*, 2)[1]), since the quadratic interaction didn't yield any significant results after FDR correction.

In the case of the deformation-based morphometry analysis, we assessed statistical significance by fitting an LME model at each voxel using the RMINC/v1.5.3.0 package for R (Lerch et al., 2017). The model used baseline-centered log-transformed absolute Jacobian determinants as the dependent variable, an interaction term between group and age in days (modeled as a quadratic polynomial), sex as an independent variable, and a random intercept allowed per mouse (*baseline-centered log-Jacobian* ~ *Group**poly(*Age*,2) + *Sex* + (*1*|*ID*)). Centering was performed by subtracting the group-specific baseline mean, such that model estimates represent deviations from baseline. Data from the three time points were included. The model outputs were corrected for

932 multiple comparisons with False Discovery Rate (FDR), with results being displayed with a 10%
933 threshold, meaning that among the voxels shown as significant, <10% will be false positives.
934 Results were plotted by overlaying the statistics map on top of the population average.
935 Visualization of voxel-wise trajectories of peak voxels was done using RMINC and ggplot2. As
936 in the case of the volumetric results, the plots display the linear terms of the interaction between
937 group and age in days (*Group**poly(*Age*, 2)[1]), as the quadratic interaction didn't yield any
938 significant results.
939

940 **Partial Least Squares Analysis**

941 The output LVs were statistically assessed by permutation testing (3000 tests), and the contribution
942 of individual variables to each LV was assessed with bootstrap resampling to estimate standard
943 errors and confidence intervals (3000 samples) (McIntosh and Lobaugh, 2004). Bootstrap is a
944 statistical resampling technique that creates several samples (with replacement) from the original
945 dataset to assess the variability of the analysis. The bootstrap ratio (BSR) is calculated as the
946 original weight/loading derived from the PLS, divided by the standard error of the weights or
947 loadings obtained from the bootstrap resampling. A BSR is frequently compared with a standard
948 normal distribution (e.g., a threshold of 1.95 for a 95% confidence interval) to assess significance.
949 BSRs are used to determine which brain areas significantly relate to behavioural measures within
950 an LV.
951

952 **Spatial Gene Enrichment analysis**

953

For the SGEA analysis, we used the tmodUtest function (tmod/0.46.2 package in R) to assess module enrichment. Genes were ranked based on their spatial correlation with the brain phenotype (PLS-LV3 loading map) using Spearman correlation. Gene modules (groups of genes with shared biological functions) were filtered to include only genes that were present in the gene expression data from the Allen Institute's Mouse Brain Atlas that we had available. Modules were further restricted to contain between 10 and 500 genes. For each module, we determined which of its genes appeared in the ranked list and where they fell in the ranking. This step allowed us to assess whether certain modules are enriched with highly ranked genes (i.e., genes that are strongly correlated with the phenotype). The Mann-Whitney test was used to compute a U-statistic and p-values for the ranked gene list, with further transformation to the Area Under the Curve (AUC) to measure effect size. The significance of the AUC was tested by comparing against randomized AUC null distributions (Fulcher et al., 2021), with p-values adjusted using FDR correction.

Funding

Healthy Brains Healthy Lives (CLG)

Fonds de recherche du Québec - Santé (CLG, CA, MU)

Author contributions

Conceptualization: CA, MMC

Data curation: CA

Formal analysis: CLG, CA

Investigation: CA, MP, MU, DG

Resources: MMC

Software: GAD, YY

Supervision: MMC

Visualization: CLG

Writing - original draft: CLG

Writing - review & editing: CLG, CA, MU, DG, ST, GAD, MMC

Competing interests

The authors declare they have no competing interests.

Data and materials availability

The data that support the findings of this study are openly available in Zenodo at https://doi.org/10.5281/zenodo.14907093. The repository includes raw data, scripts for the main analyses, and statistical maps generated in this study.

References

Albanese E, Launer LJ, Egger M, Prince MJ, Giannakopoulos P, Wolters FJ, Egan K. 2017. Body mass index in midlife and dementia: Systematic review and meta-regression analysis of 589,649 men and women followed in longitudinal studies. *Alzheimers Dement* **8**:165–178.

Alwan NA, Stannard S, Berrington A, Paranjothy S, Hoyle RB, Owen RK, Fraser SDS. 2024. Risk factors for ill health: How do we specify what is "modifiable"? *PLOS Global Public Health* **4**:e0002887.

Anastassiadis C. 2020. Effects of a high-fat diet and an exercise-based rescue on neuroanatomy in the triple-transgenic mouse model of Alzheimer's disease.

Antunes M, Biala G. 2012. The novel object recognition memory: Neurobiology, test procedure, and its modifications. *Cognitive Processing*. doi:10.1007/s10339-011-0430-z

Arel-Bundock V. 2025. Model to Meaning: How to Interpret Statistical Models with R and Python. CRC Press.

Arnatkevičiūtė A, Fulcher BD, Fornito A. 2019. A practical guide to linking brain-wide gene expression and neuroimaging data. *Neuroimage* **189**:353–367.

Avants BB, Tustison NJ, Song G, Cook PA, Klein A, Gee JC. 2011. A Reproducible Evaluation of ANTs

Similarity Metric Performance in Brain Image Registration. *Neuroimage* **54**:2033.
Avants BB, Tustison N, Song G, Others. 2009. Advanced normalization tools (ANTS). *Insight J* **2**:1–35.
Baumgart M, Snyder HM, Carrillo MC, Fazio S, Kim H, Johns H. 2015. Summary of the evidence on modifiable risk factors for cognitive decline and dementia: A population-based perspective. *Alzheimers Dement* **11**:718–726.
Belfiore R, Rodin A, Ferreira E, Velazquez R, Branca C, Caccamo A, Oddo S. 2019. Temporal and regional progression of Alzheimer's disease-like pathology in 3xTg-AD mice. *Aging Cell* **18**. doi:10.1111/ACEL.12873
Benjamini Y, Yekutieli D. 2001. The Control of the False Discovery Rate in Multiple Testing under Dependency. *Ann Stat* **29**:1165–1188.
Billings LM, Oddo S, Green KN, McGaugh JL, LaFerla FM. 2005. Intraneuronal Abeta causes the onset of early Alzheimer's disease-related cognitive deficits in transgenic mice. *Neuron* **45**:675–688.
Bromley-Brits K, Deng Y, Song W. 2011. Morris Water Maze test for learning and memory deficits in Alzheimer's disease model mice. *J Vis Exp*. doi:10.3791/2920
Brown BM, de Frutos Lucas J, Porter T, Frost N, Vacher M, Peiffer JJ, Laws SM. 2022. Non-Modifiable Factors as Moderators of the Relationship Between Physical Activity and Brain Volume: A Cross-Sectional UK Biobank Study. *J Alzheimers Dis* **88**:1091–1101.
Busenbark JR, Graffin SD, Campbell RJ, Lee EY. 2022. A marginal effects approach to interpreting main effects and moderation. *Organ Res Methods* **25**:147–169.
Bussy A, Levy JP, Best T, Patel R, Cupo L, Van Langenhove T, Nielsen JE, Pijnenburg Y, Waldö ML, Remes AM, Schroeter ML, Santana I, Pasquier F, Otto M, Danek A, Levin J, Le Ber I, Vandenberghe R, Synofzik M, Moreno F, de Mendonça A, Sanchez-Valle R, Laforce R, Langheinrich T, Gerhard A, Graff C, Butler CR, Sorbi S, Jiskoot L, Seelaar H, van Swieten JC, Finger E, Tartaglia MC, Masellis M, Tiraboschi P, Galimberti D, Borroni B, Rowe JB, Bocchetta M, Rohrer JD, Devenyi GA, Chakravarty MM, Ducharme S, GENetic Frontotemporal dementia Initiative (GENFI). 2023. Cerebellar and subcortical atrophy contribute to psychiatric symptoms in frontotemporal dementia. *Hum Brain Mapp* **44**:2684–2700.
Cahill LS, Steadman PE, Jones CE, Laliberté CL, Dazai J, Lerch JP, Stefanovic B, Sled JG. 2015. MRI-detectable changes in mouse brain structure induced by voluntary exercise. *Neuroimage* **113**:175–183.
Camiletti-Moirón D, Aparicio VA, Aranda P, Radak Z. 2013. Does exercise reduce brain oxidative stress? A systematic review. *Scand J Med Sci Sports* **23**:e202–12.
Chakravarty MM, Steadman P, van Eede MC, Calcott RD, Gu V, Shaw P, Raznahan A, Collins DL, Lerch JP. 2013. Performing label-fusion-based segmentation using multiple automatically generated templates. *Hum Brain Mapp* **34**:2635–2654.
Chung MK, Worsley KJ, Paus T, Cherif C, Collins DL, Giedd JN, Rapoport JL, Evans AC. 2001. A Unified Statistical Approach to Deformation-Based Morphometry. doi:10.1006/nimg.2001.0862
Clinton LK, Billings LM, Green KN, Caccamo A, Ngo J, Oddo S, McGaugh JL, LaFerla FM. 2007. Age-dependent sexual dimorphism in cognition and stress response in the 3xTg-AD mice. *Neurobiol Dis* **28**:76–82.
Cottam NC, Ofori K, Stoll KT, Bryant M, Rogge JR, Hekmatyar K, Sun J, Charvet CJ. 2025. From Circuits to Lifespan: Translating Mouse and Human Timelines with Neuroimaging-Based Tractography. *J Neurosci* **45**. doi:10.1523/JNEUROSCI.1429-24.2025
Coupe P, Yger P, Prima S, Hellier P, Kervrann C, Barillot C. 2008. An optimized blockwise nonlocal means denoising filter for 3-D magnetic resonance images. *IEEE Trans Med Imaging* **27**:425–441.
Cramer RD III. 1993. Partial Least Squares (PLS): Its strengths and limitations. *Perspect Drug Discov Des* **1**:269–278.
Danyluik M, Zeighami Y, Mukora A, Lepage M, Shah J, Joober R, Misic B, Iturria-Medina Y, Chakravarty MM. 2024. Evaluating permutation-based inference for partial least squares analysis of neuroimaging data. *bioRxiv*. doi:10.1101/2024.08.02.606412
Dorr AE, Lerch JP, Spring S, Kabani N, Henkelman RM. 2008. High resolution three-dimensional brain

atlas using an average magnetic resonance image of 40 adult C57Bl/6J mice. *Neuroimage* **42**:60–69.
Duff K, Eckman C, Zehr C, Yu X, Prada C-M, Perez-tur J, Hutton M, Buee L, Harigaya Y, Yager D, Morgan D, Gordon MN, Holcomb L, Refolo L, Zenk B, Hardy J, Younkin S. 1996. Increased amyloid-β42(43) in brains of mice expressing mutant presenilin 1. *Nature* **383**:710–713.
EMBL-EBI. n.d. QuickGO. https://www.ebi.ac.uk/QuickGO/GTerm?id=GO:0071333
Esquerda-Canals G, Marti J, Rivera-Hernández G, Giménez-Llort L, Villegas S. 2013. Loss of deep cerebellar nuclei neurons in the 3xTg-AD mice and protection by an anti-amyloid β antibody fragment. *MAbs* **5**:660–664.
Fernandes DJ, Ellegood J, Askalan R, Blakely RD, Dicicco-Bloom E, Egan SE, Osborne LR, Powell CM, Raznahan A, Robins DM, Salter MW, Sengar AS, Veenstra-VanderWeele J, Henkelman RM, Lerch JP. 2017. Spatial gene expression analysis of neuroanatomical differences in mouse models. *Neuroimage* **163**:220–230.
Fjell AM, Walhovd KB, Westlye LT, Østby Y, Tamnes CK, Jernigan TL, Gamst A, Dale AM. 2010. When does brain aging accelerate? Dangers of quadratic fits in cross-sectional studies. *Neuroimage* **50**:1376–1383.
Ford ES, Dietz WH. 2013. Trends in energy intake among adults in the United States: findings from NHANES. *Am J Clin Nutr* **97**:848–853.
Friedel M, van Eede MC, Pipitone J, Mallar Chakravarty M, Lerch JP. 2014. Pydpiper: A flexible toolkit for constructing novel registration pipelines. *Front Neuroinform* **8**:67.
Fulcher BD, Arnatkeviciute A, Fornito A. 2021. Overcoming false-positive gene-category enrichment in the analysis of spatially resolved transcriptomic brain atlas data. *Nat Commun* **12**:2669.
Gale SA, Acar D, Daffner KR. 2018. Dementia. *Am J Med* **131**:1161–1169.
Gallino D, Devenyi GA, Germann J, Guma E, Anastassiadis C, Chakravarty MM. 2019. Longitudinal assessment of the neuroanatomical consequences of deep brain stimulation: Application of fornical DBS in an Alzheimer's mouse model. *Brain Res* **1715**:213–223.
Gama Sosa MA, Gasperi RD, Rocher AB, Wang AC-J, Janssen WGM, Flores T, Perez GM, Schmeidler J, Dickstein DL, Hof PR, Elder GA. 2010. Age-related vascular pathology in transgenic mice expressing presenilin 1-associated familial Alzheimer's disease mutations. *Am J Pathol* **176**:353–368.
García-García I, Michaud A, Dadar M, Zeighami Y, Neseliler S, Collins DL, Evans AC, Dagher A. 2019. Neuroanatomical differences in obesity: meta-analytic findings and their validation in an independent dataset. *Int J Obes* **43**:943–951.
Gene Ontology Consortium. 2015. Gene Ontology Consortium: going forward. *Nucleic Acids Res* **43**:D1049–56.
Gerlach RW, Kowalski BR, Wold HOA. 1979. Partial least-squares path modelling with latent variables. *Anal Chim Acta* **112**:417–421.
Germann J, Gouveia FV, Chakravarty MM, Devenyi GA. 2025. Longitudinal deformation-based morphometry pipeline to study neuroanatomical differences in structural MRI based on SyN unbiased templates. *Aperture Neuro* **5**. doi:10.52294/001c.133510
Goh J, Ladiges W. 2015. Voluntary Wheel Running in Mice. *Curr Protoc Mouse Biol* **5**:283–290.
Gómez-Apo E, Mondragón-Maya A, Ferrari-Díaz M, Silva-Pereyra J. 2021. Structural Brain Changes Associated with Overweight and Obesity. *J Obes* **2021**:6613385.
Gondim OS, de Camargo VTN, Gutierrez FA, Martins PF de O, Passos MEP, Momesso CM, Santos VC, Gorjão R, Pithon-Curi TC, Cury-Boaventura MF. 2015. Benefits of regular exercise on inflammatory and cardiovascular risk markers in normal weight, overweight and obese adults. *PLoS One* **10**:e0140596.
González Olmo BM, Bettes MN, DeMarsh JW, Zhao F, Askwith C, Barrientos RM. 2023. Short-term high-fat diet consumption impairs synaptic plasticity in the aged hippocampus via IL-1 signaling. *Npj Sci Food* **7**:35.
Gray-Donald K, Jacobs-Starkey L, Johnson-Down L. 2000. Food habits of Canadians: reduction in fat intake over a generation. *Can J Public Health* **91**:381–385.

1109 Guma E, Bordignon P do C, Devenyi GA, Gallino D, Anastassiadis C, Cvetkovska V, Barry A, Snook E,
1110 Germann J, Greenwood CMT, Misic B, Bagot RC, Chakravarty MM. 2021. Early or late gestational
1111 exposure to maternal immune activation alters neurodevelopmental trajectories in mice: an
1112 integrated neuroimaging, behavioural, and transcriptional study. *Biol Psychiatry*.
1113 doi:10.1016/j.biopsych.2021.03.017
1114 Herrmann MJ, Tesar A-K, Beier J, Berg M, Warrings B. 2019. Grey matter alterations in obesity: A meta-
1115 analysis of whole-brain studies. *Obes Rev* **20**:464–471.
1116 Hörder H, Johansson L, Guo X, Grimby G, Kern S, Skoog I. 2018. Author response: Midlife
1117 cardiovascular fitness and dementia: A 44-year longitudinal population study in women. *Neurology*
1118 **91**:763.
1119 Huang H, Wang L, Cao M, Marshall C, Gao J, Xiao N, Hu G, Xiao M. 2015. Isolation Housing
1120 Exacerbates Alzheimer's Disease-Like Pathophysiology in Aged APP/PS1 Mice. *Int J*
1121 *Neuropsychopharmacol* **18**:yu116.
1122 Huang S-Y, Li Y-Z, Zhang Y-R, Huang Y-Y, Wu B-S, Zhang W, Deng Y-T, Chen S-D, He X-Y, Chen
1123 S-F, Dong Q, Zhang C, Chen R-J, Suckling J, Rolls ET, Feng J-F, Cheng W, Yu J-T. 2022. Sleep,
1124 physical activity, sedentary behavior, and risk of incident dementia: a prospective cohort study of
1125 431,924 UK Biobank participants. *Mol Psychiatry* **27**:4343–4354.
1126 Iosif CI, Bashir ZI, Apps R, Pickford J. 2023. Cerebellar prediction and feeding behaviour. *Cerebellum*
1127 **22**:1002–1019.
1128 Iturria-Medina Y, Sotero RC, Toussaint PJ, Mateos-Pérez JM, Evans AC, Weiner MW, Aisen P, Petersen
1129 R, Jack CR, Jagust W, Trojanowki JQ, Toga AW, Beckett L, Green RC, Saykin AJ, Morris J, Shaw
1130 LM, Khachaturian Z, Sorensen G, Kuller L, Raichle M, Paul S, Davies P, Fillit H, Hefti F, Holtzman
1131 D, Mesulam MM, Potter W, Snyder P, Schwartz A, Montine T, Thomas RG, Donohue M, Walter S,
1132 Gessert D, Sather T, Jiminez G, Harvey D, Bernstein M, Fox N, Thompson P, Schuff N, Borowski
1133 B, Gunter J, Senjem M, Vemuri P, Jones D, Kantarci K, Ward C, Koeppe RA, Foster N, Reiman
1134 EM, Chen K, Mathis C, Landau S, Cairns NJ, Householder E, Taylor-Reinwald L, Lee V, Korecka
1135 M, Figurski M, Crawford K, Neu S, Foroud TM, Potkin S, Shen L, Faber K, Kim S, Nho K, Thal L,
1136 Buckholtz N, Albert M, Frank R, Hsiao J, Kaye J, Quinn J, Lind B, Carter R, Dolen S, Schneider LS,
1137 Pawluczyk S, Beccera M, Teodoro L, Spann BM, Brewer J, Vanderswag H, Fleisher A, Heidebrink
1138 JL, Lord JL, Mason SS, Albers CS, Knopman D, Johnson K, Doody RS, Villanueva-Meyer J,
1139 Chowdhury M, Rountree S, Dang M, Stern Y, Honig LS, Bell KL, Ances B, Carroll M, Leon S,
1140 Mintun MA, Schneider S, Oliver A, Marson D, Griffith R, Clark D, Geldmacher D, Brockington J,
1141 Roberson E, Grossman H, Mitsis E, De Toledo-Morrell L, Shah RC, Duara R, Varon D, Greig MT,
1142 Roberts P, Albert M, Onyike C, D'Agostino D, Kielb S, Galvin JE, Cerbone B, Michel CA, Rusinek
1143 H, De Leon MJ, Glodzik L, De Santi S, Doraiswamy PM, Petrella JR, Wong TZ, Arnold SE,
1144 Karlawish JH, Wolk D, Smith CD, Jicha G, Hardy P, Sinha P, Oates E, Conrad G, Lopez OL,
1145 Oakley M, Simpson DM, Porsteinsson AP, Goldstein BS, Martin K, Makino KM, Ismail MS, Brand
1146 C, Mulnard RA, Thai G, Mc-Adams-Ortiz C, Womack K, Mathews D, Quiceno M, Diaz-Arrastia R,
1147 King R, Weiner M, Martin-Cook K, DeVous M, Levey AI, Lah JJ, Cellar JS, Burns JM, Anderson
1148 HS, Swerdlow RH, Apostolova L, Tingus K, Woo E, Silverman DHS, Lu PH, Bartzokis G, Graff-
1149 Radford NR, Parfitt F, Kendall T, Johnson H, Farlow MR, Hake A, Matthews BR, Herring S, Hunt
1150 C, Van Dyck CH, Carson RE, MacAvoy MG, Chertkow H, Bergman H, Hosein C, Black S,
1151 Stefanovic B, Caldwell C, Hsiung GYR, Feldman H, Mudge B, Assaly M, Kertesz A, Rogers J,
1152 Bernick C, Munic D, Kerwin D, Mesulam MM, Lipowski K, Wu CK, Johnson N, Sadowsky C,
1153 Martinez W, Villena T, Turner RS, Johnson K, Reynolds B, Sperling RA, Johnson KA, Marshall G,
1154 Frey M, Lane B, Rosen A, Tinklenberg J, Sabbagh MN, Belden CM, Jacobson SA, Sirrel SA,
1155 Kowall N, Killiany R, Budson AE, Norbash A, Johnson PL, Allard J, Lerner A, Ogrocki P, Hudson
1156 L, Fletcher E, Carmichael O, Olichney J, DeCarli C, Kittur S, Borrie M, Lee TY, Bartha R, Johnson
1157 S, Asthana S, Carlsson CM, Potkin SG, Preda A, Nguyen D, Tariot P, Reeder S, Bates V, Capote H,
1158 Rainka M, Scharre DW, Kataki M, Adeli A, Zimmerman EA, Celmins D, Brown AD, Pearlson GD,
1159 Blank K, Anderson K, Santulli RB, Kitzmiller TJ, Schwartz ES, Sink KM, Williamson JD, Garg P,

Watkins F, Ott BR, Querfurth H, Tremont G, Salloway S, Malloy P, Correia S, Rosen HJ, Miller BL, Mintzer J, Spicer K, Bachman D, Finger E, Pasternak S, Rachinsky I, Drost D, Pomara N, Hernando R, Sarrael A, Schultz SK, Ponto LLB, Shim H, Smith KE, Relkin N, Chaing G, Raudin L, Smith A, Fargher K, Raj BA, Neylan T, Grafman J, Davis M, Morrison R, Hayes J, Finley S, Friedl K, Fleischman D, Arfanakis K, James O, Massoglia D, Fruehling JJ, Harding S, Peskind ER, Petrie EC, Li G, Yesavage JA, Taylor JL, Furst AJ. 2016. Early role of vascular dysregulation on late-onset Alzheimer's disease based on multifactorial data-driven analysis. *Nat Commun* **7**. doi:10.1038/ncomms11934

Jalanko P, Säisänen L, Kallioniemi E, Könönen M, Lakka TA, Määttä S, Haapala EA. 2024. Associations between physical fitness and cerebellar gray matter volume in adolescents. *Scand J Med Sci Sports* **34**:e14513.

Javonillo DI, Tran KM, Phan J, Hingco E, Kramár EA, da Cunha C, Forner S, Kawauchi S, Milinkeviciute G, Gomez-Arboledas A, Neumann J, Banh CE, Huynh M, Matheos DP, Rezaie N, Alcantara JA, Mortazavi A, Wood MA, Tenner AJ, MacGregor GR, Green KN, LaFerla FM. 2022. Systematic Phenotyping and Characterization of the 3xTg-AD Mouse Model of Alzheimer's Disease. *Front Neurosci* **15**. doi:10.3389/fnins.2021.785276

Jensen DEA, Leoni V, Klein-Flügge MC, Ebmeier KP, Suri S. 2021. Associations of dietary markers with brain volume and connectivity: A systematic review of MRI studies. *Ageing Res Rev* **70**:101360.

Jullienne A, Trinh MV, Obenaus A. 2022. Neuroimaging of mouse models of Alzheimer's Disease. *Biomedicines* **10**:305.

Khan S, Barve KH, Kumar MS. 2020. Recent Advancements in Pathogenesis, Diagnostics and Treatment of Alzheimer's Disease. *Curr Neuropharmacol* **18**:1106–1125.

Kim D, Cho J, Lee I, Jin Y, Kang H. 2017. Exercise Attenuates High-Fat Diet-induced Disease Progression in 3xTg-AD Mice. *Med Sci Sports Exerc* **49**:676–686.

Knight EM, Martins IVA, Gümüsgöz S, Allan SM, Lawrence CB. 2014. High-fat diet-induced memory impairment in triple-transgenic Alzheimer's disease (3xTgAD) mice is independent of changes in amyloid and tau pathology. *Neurobiol Aging* **35**:1821–1832.

Knowler WC, Narayan KMV, Hanson RL, Nelson RG, Bennett PH, Tuomilehto J, Schersten B, Pettitt DJ. 1995. Preventing non-insulin-dependent diabetes. *Diabetes* **44**:483–488.

Kong V, Devenyi GA, Gallino D, Ayranci G, Germann J, Rollins C, Chakravarty MM. 2018. Early-in-life neuroanatomical and behavioural trajectories in a triple transgenic model of Alzheimer's disease. *Brain Struct Funct* **223**:3365–3382.

Koziol LF, Budding D, Andreasen N, D'Arrigo S, Bulgheroni S, Imamizu H, Ito M, Manto M, Marvel C, Parker K, Pezzulo G, Ramnani N, Riva D, Schmahmann J, Vandervert L, Yamazaki T. 2014. Consensus paper: the cerebellum's role in movement and cognition. *Cerebellum* **13**:151–177.

Kuo YT, Herlihy AH, So PW, Bhakoo KK, Bell JD. 2005. In vivo measurements of T1 relaxation times in mouse brain associated with different modes of systemic administration of manganese chloride. *J Magn Reson Imaging* **21**:334–339.

Lai M, Chandrasekera PC, Barnard ND. 2014. You are what you eat, or are you? The challenges of translating high-fat-fed rodents to human obesity and diabetes. *Nutr Diabetes* **4**:e135.

Lau JC, Lerch JP, Sled JG, Henkelman RM, Evans AC, Bedell BJ. 2008. Longitudinal neuroanatomical changes determined by deformation-based morphometry in a mouse model of Alzheimer's disease. *Neuroimage* **42**:19–27.

Lee JH, Silva AC, Merkle H, Koretsky AP. 2005. Manganese-enhanced magnetic resonance imaging of mouse brain after systemic administration of MnCl2: Dose-dependent and temporal evolution of T1 contrast. *Magn Reson Med* **53**:640–648.

Lein ES, Hawrylycz MJ, Ao N, Ayres M, Bensinger A, Bernard A, Boe AF, Boguski MS, Brockway KS, Byrnes EJ, Chen L, Chen L, Chen T-M, Chin MC, Chong J, Crook BE, Czaplinska A, Dang CN, Datta S, Dee NR, Desaki AL, Desta T, Diep E, Dolbeare TA, Donelan MJ, Dong H-W, Dougherty JG, Duncan BJ, Ebbert AJ, Eichele G, Estin LK, Faber C, Facer BA, Fields R, Fischer SR, Fliss TP, Frensley C, Gates SN, Glattfelder KJ, Halverson KR, Hart MR, Hohmann JG, Howell MP, Jeung

1211 DP, Johnson RA, Karr PT, Kawal R, Kidney JM, Knapik RH, Kuan CL, Lake JH, Laramee AR,
1212 Larsen KD, Lau C, Lemon TA, Liang AJ, Liu Y, Luong LT, Michaels J, Morgan JJ, Morgan RJ,
1213 Mortrud MT, Mosqueda NF, Ng LL, Ng R, Orta GJ, Overly CC, Pak TH, Parry SE, Pathak SD,
1214 Pearson OC, Puchalski RB, Riley ZL, Rockett HR, Rowland SA, Royall JJ, Ruiz MJ, Sarno NR,
1215 Schaffnit K, Shapovalova NV, Sivisay T, Slaughterbeck CR, Smith SC, Smith KA, Smith BI, Sodt
1216 AJ, Stewart NN, Stumpf K-R, Sunkin SM, Sutram M, Tam A, Teemer CD, Thaller C, Thompson
1217 CL, Varnam LR, Visel A, Whitlock RM, Wohnoutka PE, Wolkey CK, Wong VY, Wood M,
1218 Yaylaoglu MB, Young RC, Youngstrom BL, Yuan XF, Zhang B, Zwingman TA, Jones AR. 2007.
1219 Genome-wide atlas of gene expression in the adult mouse brain. *Nature* **445**:168–176.
1220 Lerch J, Hammill C, van Eede M, Cassel D, Nikelski J, Yee Y, Friedel M, Wang N, Devenyi G. 2017.
1221 RMINC: Statistical Tools for Medical Imaging NetCDF (MINC) Files.
1222 Lewis J, McGowan E, Rockwood J, Melrose H, Nacharaju P, Van Slegtenhorst M, Gwinn-Hardy K,
1223 Murphy MP, Baker M, Yu X, Duff K, Hardy J, Corral A, Lin WL, Yen SH, Dickson DW, Davies P,
1224 Hutton M. 2000. Neurofibrillary tangles, amyotrophy and progressive motor disturbance in mice
1225 expressing mutant (P301L)tau protein. *Nat Genet* **25**:402–405.
1226 Lindqvist A, Mohapel P, Bouter B, Frielingsdorf H, Pizzo D, Brundin P, Erlanson-Albertsson C. 2006.
1227 High-fat diet impairs hippocampal neurogenesis in male rats. *Eur J Neurol* **13**:1385–1388.
1228 Liśkiewicz A, Przybyła M, Wojakowska A, Marczak Ł, Bogus K, Nowacka-Chmielewska M, Liśkiewicz
1229 D, Małecki A, Barski J, Lewin-Kowalik J, Toborek M. 2020. Physical activity reduces anxiety and
1230 regulates brain fatty acid synthesis. *Mol Brain* **13**:62.
1231 Liu Z, Whitaker KJ, Smith SM, Nichols TE. 2022. Improved interpretability of brain-behavior CCA with
1232 Domain-driven Dimension Reduction. *Front Neurosci* **16**:851827.
1233 Livingston G, Huntley J, Liu KY, Costafreda SG, Selbæk G, Alladi S, Ames D, Banerjee S, Burns A,
1234 Brayne C, Fox NC, Ferri CP, Gitlin LN, Howard R, Kales HC, Kivimäki M, Larson EB, Nakasujja
1235 N, Rockwood K, Samus Q, Shirai K, Singh-Manoux A, Schneider LS, Walsh S, Yao Y, Sommerlad
1236 A, Mukadam N. 2024. Dementia prevention, intervention, and care: 2024 report of the Lancet
1237 standing Commission. *Lancet* **404**:572–628.
1238 Livingston G, Huntley J, Sommerlad A, Ames D, Ballard C, Banerjee S, Brayne C, Burns A, Cohen-
1239 Mansfield J, Cooper C, Costafreda SG, Dias A, Fox N, Gitlin LN, Howard R, Kales HC, Kivimäki
1240 M, Larson EB, Ogunniyi A, Orgeta V, Ritchie K, Rockwood K, Sampson EL, Samus Q, Schneider
1241 LS, Selbæk G, Teri L, Mukadam N. 2020. Dementia prevention, intervention, and care: 2020 report
1242 of the Lancet Commission. *Lancet* **396**:413–446.
1243 Lueptow LM. 2017. Novel object recognition test for the investigation of learning and memory in mice. *J*
1244 *Vis Exp* **2017**:55718.
1245 Macedo RCO, Santos HO, Tinsley GM, Reischak-Oliveira A. 2020. Low-carbohydrate diets: Effects on
1246 metabolism and exercise - A comprehensive literature review. *Clin Nutr ESPEN* **40**:17–26.
1247 Maei HR, Zaslavsky K, Teixeira CM, Frankland PW. 2009. What is the most sensitive measure of water
1248 maze probe test performance? *Front Integr Neurosci* **3**:4.
1249 Maesako M, Uemura K, Kubota M, Kuzuya A, Sasaki K, Hayashida N, Asada-Utsugi M, Watanabe K,
1250 Uemura M, Kihara T, Takahashi R, Shimohama S, Kinoshita A. 2012. Exercise is more effective
1251 than diet control in preventing high fat diet-induced β-amyloid deposition and memory deficit in
1252 amyloid precursor protein transgenic mice. *J Biol Chem* **287**:23024–23033.
1253 Martins IVA, Rivers-Auty J, Allan SM, Lawrence CB. 2017. Mitochondrial abnormalities and synaptic
1254 loss underlie memory deficits seen in mouse models of obesity and Alzheimer's disease. *J*
1255 *Alzheimers Dis* **55**:915–932.
1256 McCoy KD, Geuking MB, Ronchi F. 2017. Gut Microbiome Standardization in Control and Experimental
1257 Mice. *Curr Protoc Immunol* **117**:23.1.1–23.1.13.
1258 McIntosh AR, Bookstein FL, Haxby JV, Grady CL. 1996. Spatial pattern analysis of functional brain
1259 images using partial least squares. *Neuroimage* **3**:143–157.
1260 McIntosh AR, Lobaugh NJ. 2004. Partial least squares analysis of neuroimaging data: applications and
1261 advances. *Neuroimage* **23 Suppl 1**:S250–63.

McIntosh AR, Mišić B. 2013. Multivariate statistical analyses for neuroimaging data. *Annual Review of Psychology*. doi:10.1146/annurev-psych-113011-143804

Milanski M, Degasperi G, Coope A, Morari J, Denis R, Cintra DE, Tsukumo DML, Anhe G, Amaral ME, Takahashi HK, Curi R, Oliveira HC, Carvalheira JBC, Bordin S, Saad MJ, Velloso LA. 2009. Saturated fatty acids produce an inflammatory response predominantly through the activation of TLR4 signaling in hypothalamus: implications for the pathogenesis of obesity. *J Neurosci* **29**:359–370.

Molteni R, Wu A, Vaynman S, Ying Z, Barnard RJ, Gómez-Pinilla F. 2004. Exercise reverses the harmful effects of consumption of a high-fat diet on synaptic and behavioral plasticity associated to the action of brain-derived neurotrophic factor. *Neuroscience* **123**:429–440.

Niccoli T, Partridge L. 2012. Ageing as a risk factor for disease. *Curr Biol* **22**:R741–52.

Oddo S, Caccamo A, Shepherd JD, Murphy MP, Golde TE, Kayed R, Metherate R, Mattson MP, Akbari Y, LaFerla FM. 2003. Triple-transgenic model of Alzheimer's disease with plaques and tangles: intracellular Abeta and synaptic dysfunction. *Neuron* **39**:409–421.

Ou X, Andres A, Pivik RT, Cleves MA, Badger TM. 2015. Brain gray and white matter differences in healthy normal weight and obese children. *J Magn Reson Imaging* **42**:1205–1213.

Pearce AL, Fuchs B, Adise S, Masterson TD, Fearnbach N, English L, Keller KL. 2023. Loss of control eating in children is associated with altered cortical and subcortical brain structure. *Front Psychol* **14**:1237591.

Pereira IT, Burwell RD. 2015. Using the spatial learning index to evaluate performance on the water maze. *Behav Neurosci* **129**:533–539.

Raji CA, Meysami S, Hashemi S, Garg S, Akbari N, Ahmed G, Chodakiewitz YG, Nguyen TD, Niotis K, Merrill DA, Attariwala R. 2024. Exercise-Related Physical Activity Relates to Brain Volumes in 10,125 Individuals. *J Alzheimers Dis* **97**:829–839.

Rännar S, Lindgren F, Geladi P, Wold S. 1994. A PLS kernel algorithm for data sets with many variables and fewer objects. Part 1: Theory and algorithm. *J Chemom* **8**:111–125.

Redila VA, Christie BR. 2006. Exercise-induced changes in dendritic structure and complexity in the adult hippocampal dentate gyrus. *Neuroscience* **137**:1299–1307.

Reijnders MJMF, Waterhouse RM. 2021. Summary visualizations of Gene Ontology terms with GO-Figure! *Front Bioinform* **1**:638255.

Ren Y, Savadlou A, Park S, Siska P, Epp JR, Sargin D. 2023. The impact of loneliness and social isolation on the development of cognitive decline and Alzheimer's Disease. *Front Neuroendocrinol* **69**:101061.

Rexrode KM, Manson JE, Hennekens CH. 1996. Obesity and cardiovascular disease. *Curr Opin Cardiol* **11**:490–495.

Richards K, Watson C, Buckley RF, Kurniawan ND, Yang Z, Keller MD, Beare R, Bartlett PF, Egan GF, Galloway GJ, Paxinos G, Petrou S, Reutens DC. 2011. Segmentation of the mouse hippocampal formation in magnetic resonance images. *Neuroimage* **58**:732–740.

Rollins CPE, Gallino D, Kong V, Ayranci G, Devenyi GA, Germann J, Chakravarty MM. 2019. Contributions of a high-fat diet to Alzheimer's disease-related decline: A longitudinal behavioural and structural neuroimaging study in mouse models. *NeuroImage: Clinical* **21**. doi:10.1016/j.nicl.2018.11.016

Sadleir KR, Eimer WA, Cole SL, Vassar R. 2015. Aβ reduction in BACE1 heterozygous null 5XFAD mice is associated with transgenic APP level. *Mol Neurodegener* **10**:1.

Sah SK, Lee C, Jang J-H, Park GH. 2017. Effect of high-fat diet on cognitive impairment in triple-transgenic mice model of Alzheimer's disease. *Biochem Biophys Res Commun* **493**:731–736.

Scarmeas N, Luchsinger JA, Schupf N, Brickman AM, Cosentino S, Tang MX, Stern Y. 2009. Physical activity, diet, and risk of Alzheimer disease. *JAMA* **302**:627–637.

Seo Y, Satoh K, Watanabe K, Morita H, Takamata A, Ogino T, Murakami M. 2011. Mn-bicine: A low affinity chelate for manganese ion enhanced MRI. *Magn Reson Med* **65**:1005–1012.

Souza J, da Silva RA, da Luz Scheffer D, Penteado R, Solano A, Barros L, Budde H, Trostchansky A,

1313 Latini A. 2022. Physical-exercise-induced antioxidant effects on the brain and skeletal muscle.
1314 *Antioxidants (Basel)* **11**:826.
1315 Starr ME, Saito H. 2012. Age-Related Increase in Food Spilling by Laboratory Mice May Lead to
1316 Significant Overestimation of Actual Food Consumption: Implications for Studies on Dietary
1317 Restriction, Metabolism, and Dose Calculations. *J Gerontol A Biol Sci Med Sci* **67**:1043.
1318 Steadman PE, Ellegood J, Szulc KU, Turnbull DH, Joyner AL, Henkelman RM, Lerch JP. 2014. Genetic
1319 effects on cerebellar structure across mouse models of autism using a magnetic resonance imaging
1320 atlas. *Autism Res* **7**:124–137.
1321 Tang Y, Chen D, Li X. 2022. Dimensionality reduction methods for brain imaging data analysis. *ACM*
1322 *Comput Surv* **54**:1–36.
1323 Tang Y, Zhang Y, Zheng M, Chen J, Chen H, Liu N. 2018. Effects of treadmill exercise on cerebral
1324 angiogenesis and MT1-MMP expression after cerebral ischemia in rats. *Brain Behav* **8**:e01079.
1325 Tubiana M. 1999. Cancer prevention. *Acta Oncol* **38**:689–694.
1326 Tullo S, Miranda AS, Del Cid-Pellitero E, Lim MP, Gallino D, Attaran A, Patel R, Novikov V, Park M,
1327 Beraldo FH, Luo W, Shlaifer I, Durcan TM, Bussey TJ, Saksida LM, Fon EA, Prado VF, Prado
1328 MAM, Chakravarty MM. 2024. Neuroanatomical and cognitive biomarkers of alpha-synuclein
1329 propagation in a mouse model of synucleinopathy prior to onset of motor symptoms. *J Neurochem*
1330 **168**:1546–1564.
1331 Tullo S, Park J, Gallino D, Park M, Mar K, Novikov V, Sandoval Contreras R, Patel R, Del Cid-Pellitero
1332 E, Fon EA, Luo W, Shlaifer I, Durcan TM, Prado MAM, Prado VF, Devenyi GA, Chakravarty MM.
1333 2025. Female mice exhibit resistance to disease progression despite early pathology in a transgenic
1334 mouse model inoculated with alpha-synuclein fibrils. *Commun Biol* **8**:288.
1335 Tustison NJ, Avants BB, Cook PA, Zheng Y, Egan A, Yushkevich PA, Gee JC. 2010. N4ITK: Improved
1336 N3 Bias Correction. doi:10.1109/TMI.2010.2046908
1337 Ullmann JFP, Watson C, Janke AL, Kurniawan ND, Reutens DC. 2013. A segmentation protocol and
1338 MRI atlas of the C57BL/6J mouse neocortex. *Neuroimage* **78**:196–203.
1339 Vandal M, White PJ, Tremblay C, St-Amour I, Chevrier G, Emond V, Lefrançois D, Virgili J, Planel E,
1340 Giguere Y, Marette A, Calon F. 2014. Insulin reverses the high-fat diet-induced increase in brain Aβ
1341 and improves memory in an animal model of Alzheimer disease. *Diabetes* **63**:4291–4301.
1342 van Eede MC, Scholz J, Chakravarty MM, Henkelman RM, Lerch JP. 2013. Mapping registration
1343 sensitivity in MR mouse brain images. *Neuroimage* **82**:226–236.
1344 Vaynman SS, Ying Z, Yin D, Gomez-Pinilla F. 2006. Exercise differentially regulates synaptic proteins
1345 associated to the function of BDNF. *Brain Res* **1070**:124–130.
1346 Vorhees CV, Williams MT. 2006. Morris water maze: Procedures for assessing spatial and related forms
1347 of learning and memory. *Nat Protoc* **1**:848–858.
1348 Walker JM, Dixit S, Saulsberry AC, May JM, Harrison FE. 2017. Reversal of high fat diet-induced
1349 obesity improves glucose tolerance, inflammatory response, β-amyloid accumulation and cognitive
1350 decline in the APP/PSEN1 mouse model of Alzheimer's disease. *Neurobiol Dis* **100**:87–98.
1351 Wang Q, Ding SL, Li Y, Royall J, Feng D, Lesnar P, Graddis N, Naeemi M, Facer B, Ho A, Dolbeare T,
1352 Blanchard B, Dee N, Wakeman W, Hirokawa KE, Szafer A, Sunkin SM, Oh SW, Bernard A,
1353 Phillips JW, Hawrylycz M, Koch C, Zeng H, Harris JA, Ng L. 2020. The Allen Mouse Brain
1354 Common Coordinate Framework: A 3D Reference Atlas. *Cell* **181**:936–953.e20.
1355 Webster SJ, Bachstetter AD, Nelson PT, Schmitt FA, Van Eldik LJ. 2014. Using mice to model
1356 Alzheimer's dementia: an overview of the clinical disease and the preclinical behavioral changes in
1357 10 mouse models. *Front Genet* **5**:88.
1358 World Health Organization. 2021. Global status report on the public health response to dementiaSecurity
1359 Research Hub Reports.
1360 Xu C-J, Li M-Q, Li-Zhao, Chen W-G, Wang J-L. 2021. Short-term high-fat diet favors the appearances of
1361 apoptosis and gliosis by activation of ERK1/2/p38MAPK pathways in brain. *Aging* **13**:23133–
1362 23148.
1363 Yang J, Li Q. 2020. Manganese-Enhanced Magnetic Resonance Imaging: Application in Central Nervous

System Diseases. *Front Neurol* **11**:143.
Zotcheva E, Bergh S, Selbæk G, Krokstad S, Håberg AK, Strand BH, Ernstsen L. 2018. Midlife Physical Activity, Psychological Distress, and Dementia Risk: The HUNT Study. *J Alzheimers Dis* **66**:825–833.

Figures

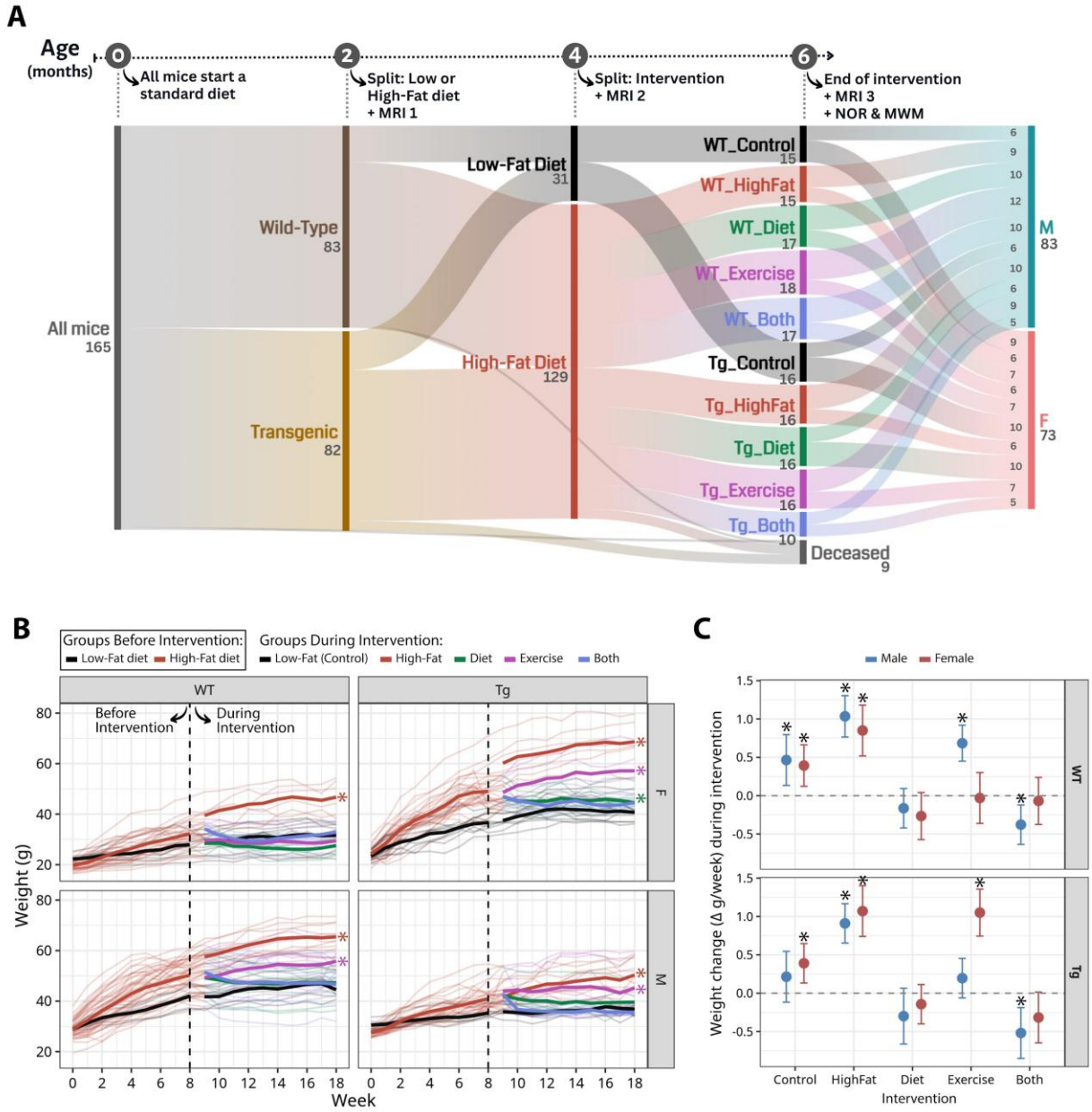

1373 **Fig. 1. Experimental design and weight changes.** (A) For the first two months, all mice received
1374 a standard diet. From two to four months of age, mice were put on either a low-fat or a high-fat
1375 diet. From four to six months of age, mice were placed in intervention groups. T1w MRIs were
1376 collected at two, four, and six months. Behavioural tests (MWM and NOR) were performed after
1377 the last MRI scan. (B) Weekly measurements of weight plotted per group. The vertical dotted line
1378 indicates the onset of interventions. The x-axis denotes time in weeks, and the y-axis body weight
1379 in grams (g). Before interventions, trajectories reflect the weight of mice maintained on a low-fat
1380 diet (black) or a high-fat diet (red). After the onset of interventions (week ≥ 8), trajectories are
1381 shown separately for each intervention group (see legend). Significant weight differences ($p <$
1382 0.05) compared against Control are denoted with an asterisk (*). (C) Model-estimated rates of
1383 weight change (g/week), stratified by intervention, genotype, and sex. Weight change was
1384 estimated using marginal contrasts derived from a four-way linear mixed effects model (*Weight* ~
1385 *Week*Intervention*Genotype*Sex* + (*Week*|*ID*)). Asterisks (*) indicate estimates with 95%
1386 confidence intervals excluding zero ($p < 0.05$), indicating a significant weight gain or loss. N =
1387 156 mice, with 18 repeated weight measurements each.
1388

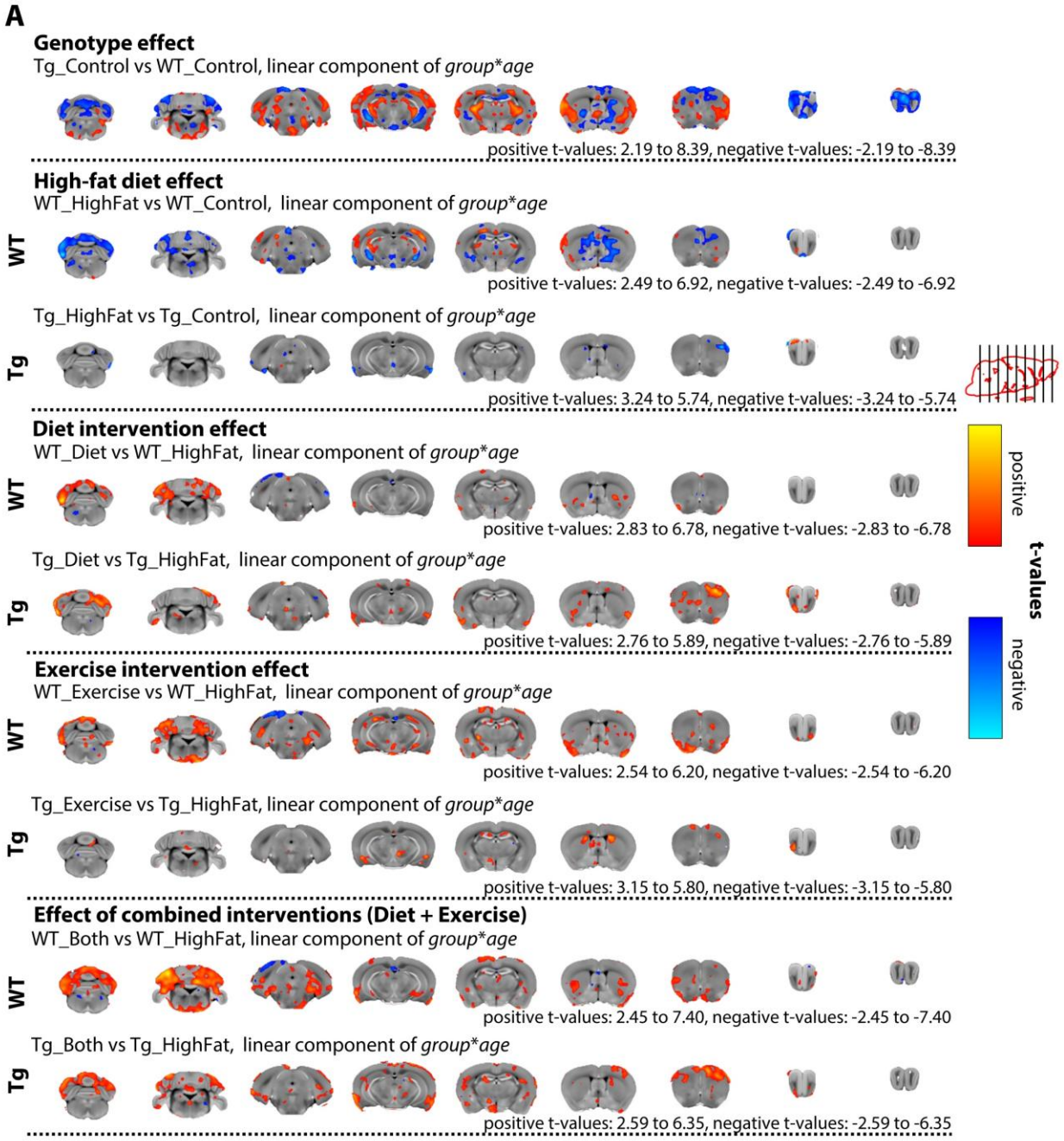

Fig. 2. Age-dependent group differences in brain volume change. The *t*-statistic maps show the linear component of the group and age interaction, thresholded at 10% FDR and displayed at their peak *t*-values, overlaid on the population-average brain. Estimates were derived from a linear mixed-effects model of the log-transformed Jacobian determinant (~ *Group* * poly(*Age*, 2) + *Sex* + (1 | ID)). N = 152 mice.

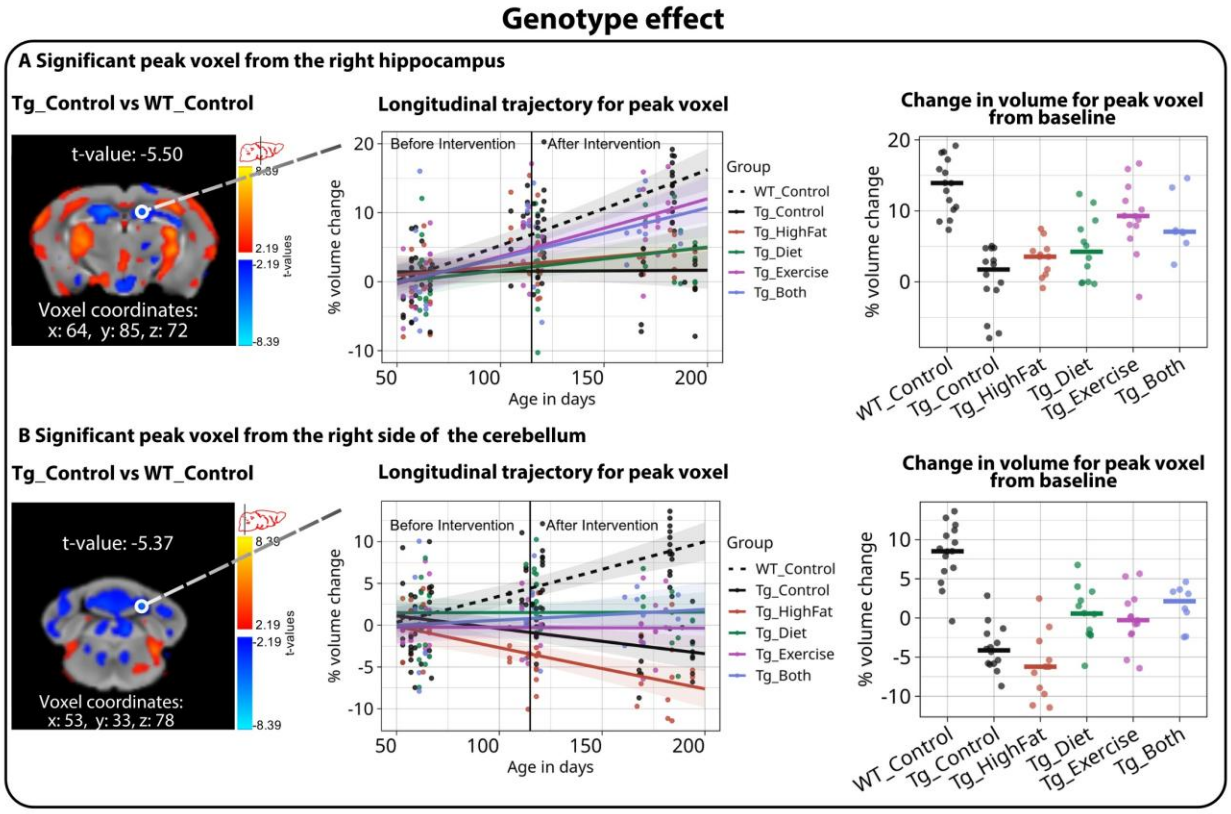

Fig. 3. Trajectories of significant peak voxels identified for the genotype effect. The figure shows peak voxels selected from the comparison between Tg_Control and WT_Control, which highlights the genotype effect on the hippocampus (A) and cerebellum (B). The left panels show the statistical maps of the interaction between the group and age in days, thresholded at 10% FDR, together with the corresponding *t*-values and voxel coordinates (from model: *log-Jacobian* ~ *Group**poly(*Age*,2) + *Sex* + (*1*|*ID*)). The middle panels show the percent change in volume from baseline in the selected peak voxels. The right panels show the percent volume change from baseline at the final time point; horizontal lines represent the group median, and individual data points are overlaid to illustrate distribution. FDR: False Discovery Rate.

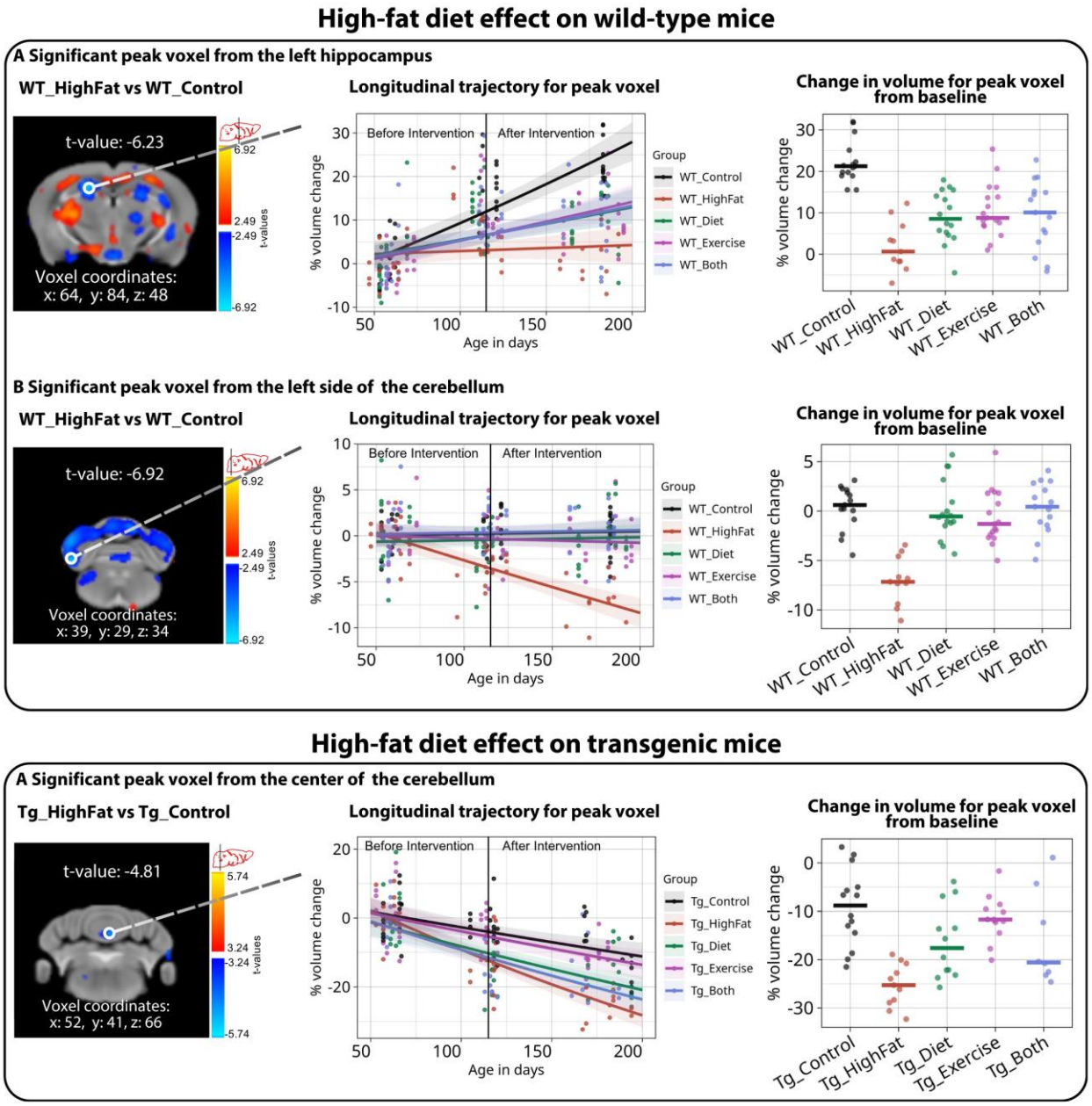

Fig. 4. Trajectories of significant peak voxels identified for the high-fat diet effect. Significant peak voxels were selected from comparisons between WT_HighFat and WT_Control (top panels, A-B) and between Tg_HighFat and Tg_Control (bottom panel, A), highlighting genotype-specific effects of the obesity-inducing high-fat diet. Left panels: statistical maps of the interaction between group and age (from model: *log-Jacobian* ~ *Group**poly(*Age*,2) + *Sex* + (*1*|*ID*), 10% FDR corrected). Middle panels: longitudinal percent change in volume from baseline across all three

time points. Right panels: percent volume change from baseline and median at the last time point. FDR: False Discovery Rate.

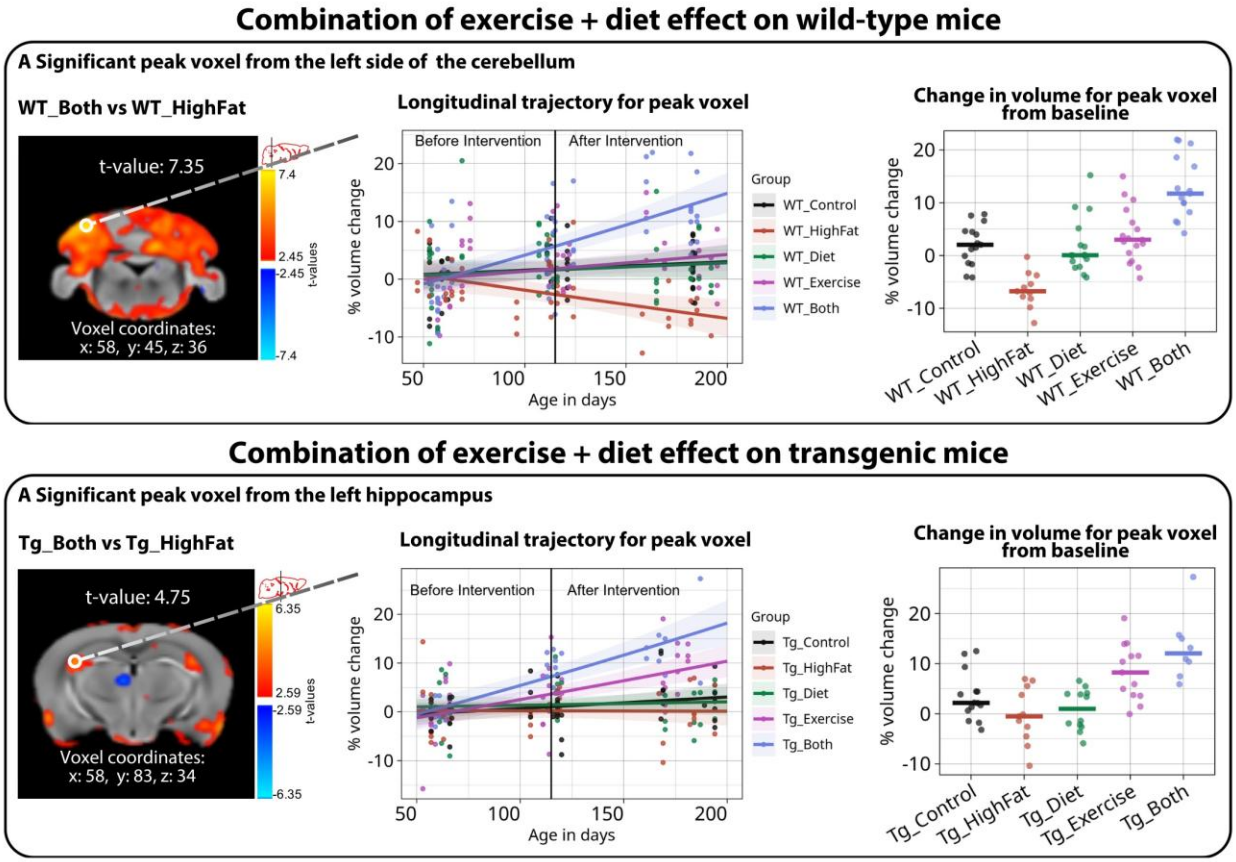

Fig. 5. Trajectories of significant peak voxels identified for the combined interventions. Significant peak voxels were selected from the left side of the cerebellum, from the comparison between WT_Both and WT_HighFat (top panel, A), and the left hippocampus from the comparison between Tg_Both and Tg_HighFat (bottom panel, A), highlighting effects of the combined exercise and diet intervention in each genotype. Panels show the statistical maps of the interaction between group and age (from model: *log-Jacobian* ~ *Group**poly(*Age*,2) + *Sex* + (*1*|*ID*), 10% FDR corrected, left panels), longitudinal percent change in volume from baseline

1425 across all three time points (middle panels), and percent volume change from baseline and the

1426 group median at the last time point (right panels). FDR: False Discovery Rate.

1427

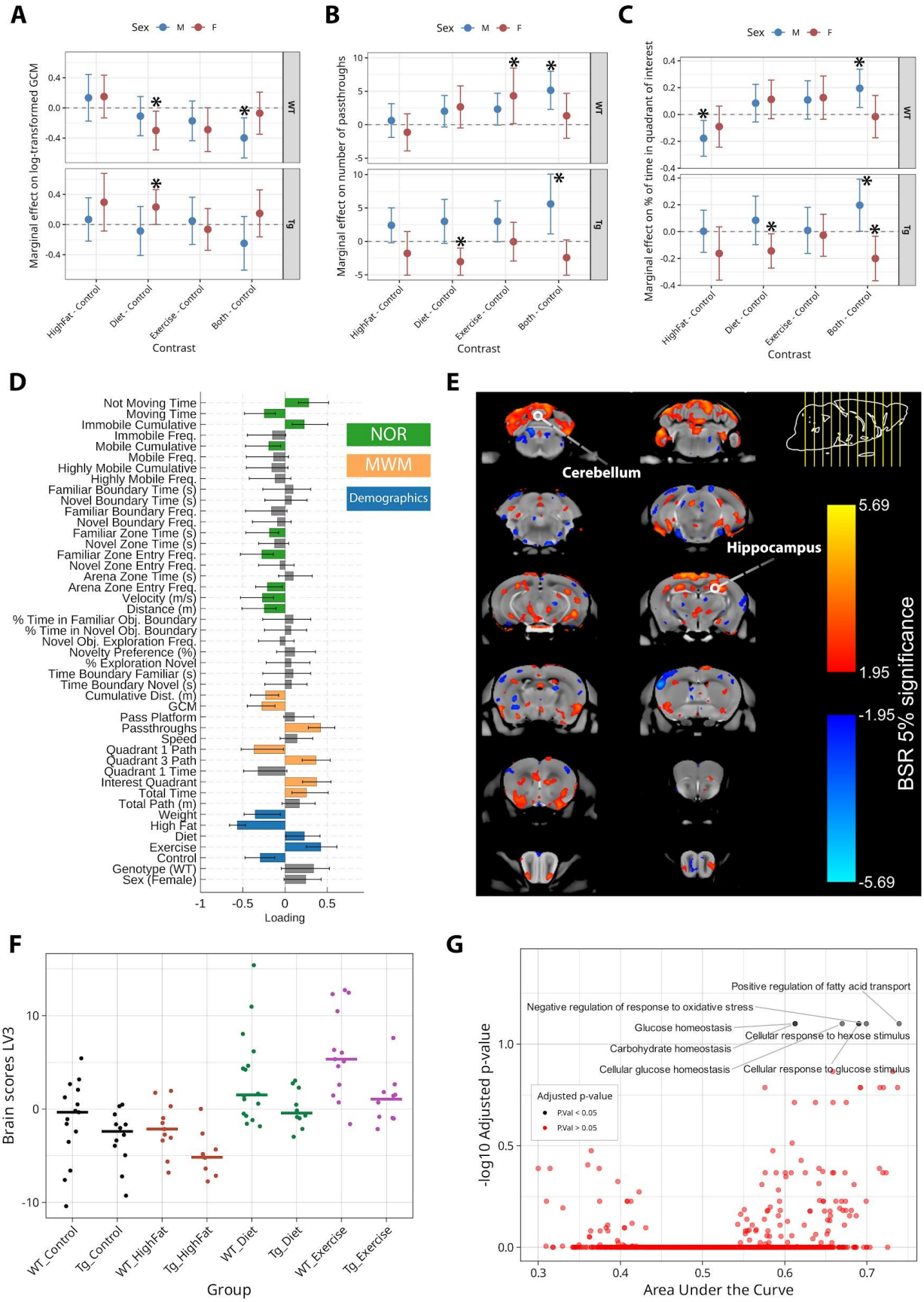
A
Sex M F
Marginal effect on log-transformed GCM
WT
Tg
HighFat - Control
Diet - Control
Exercise - Control
Both - Control
Contrast
B
Marginal effect on number of passthroughs
C
Marginal effect on % of time in quadrant of interest
D
NOR
MWM
Demographics
Not Moving Time
Moving Time
Immobile Cumulative
Immobile Freq.
Mobile Cumulative
Mobile Freq.
Highly Mobile Cumulative
Highly Mobile Freq.
Familiar Boundary Time (s)
Novel Boundary Time (s)
Familiar Boundary Freq.
Novel Boundary Freq.
Familiar Zone Time (s)
Novel Zone Time (s)
Familiar Zone Entry Freq.
Novel Zone Entry Freq.
Arena Zone Time (s)
Arena Zone Entry Freq.
Velocity (m/s)
Distance (m)
% Time in Familiar Obj. Boundary
% Time in Novel Obj. Boundary
Novel Obj. Exploration Freq.
Novelty Preference (%)
% Exploration Novel
Time Boundary Familiar (s)
Time Boundary Novel (s)
Cumulative Dist. (m)
GCM
Pass Platform
Passthroughs
Speed
Quadrant 1 Path
Quadrant 3 Path
Quadrant 1 Time
Interest Quadrant
Total Time
Total Path (m)
Weight
High Fat
Diet
Exercise
Control
Genotype (WT)
Sex (Female)
Loading
E
Cerebellum
Hippocampus
5.69
1.95
-1.95
-5.69
BSR 5% significance
F
Brain scores LV3
WT_Control
Tg_Control
WT_HighFat
Tg_HighFat
WT_Diet
Tg_Diet
WT_Exercise
Tg_Exercise
Group
G
Positive regulation of fatty acid transport
Negative regulation of response to oxidative stress
Glucose homeostasis
Cellular response to hexose stimulus
Carbohydrate homeostasis
Cellular glucose homeostasis
Cellular response to glucose stimulus
Adjusted p-value
P.Val < 0.05
P.Val > 0.05
-log10 Adjusted p-value
Area Under the Curve

1428

1429 **Fig. 6. Intervention-associated effects across behavioural outcomes, multivariate, and gene**
1430 **enrichment analyses.** (A) Marginal contrasts for log-transformed Gallagher's Cumulative
1431 Measurement (GCM), where lower GCM values indicate better learning. (B) Marginal contrasts
1432 for the number of pass-throughs, a measure of spatial memory retention; higher values indicate
1433 better performance. (C) Marginal contrasts for the percentage of time spent in the target quadrant
1434 of interest (where the platform was located during training); higher values indicate better
1435 performance. Points show contrasts comparing each intervention (HighFat, Diet, Exercise, and
1436 Both) to the Control, stratified by Genotype (WT, top; Tg, bottom) and Sex (Blue = Male, Red =
1437 Female). Error bars denote 95% confidence intervals; intervals crossing the zero line indicate non-
1438 significant differences. Tg = 3xTgAD mice. (D) shows the PLS-LV3 behavioural pattern that
1439 maximally covaries with the brain pattern (E). For the behavioural data (D), variables from the
1440 NOR (in green), the MWM (in yellow), and the treatment groups or demographics (in blue) are
1441 shown. The bars show how much each behaviour contributes to the pattern of LV3 (x-axis: loading
1442 values). Singular value decomposition estimated the size of the bars, whereas confidence intervals
1443 were estimated by bootstrapping. Bars with error bars that crossed the zero line are not significant
1444 (in gray). (E) Brain loading BSRs are overlaid on the population average. BSR thresholded to 95%
1445 confidence interval (N = 96 mice with complete data). (F) Group-wise distribution of brain scores
1446 (derived from PLS) and median, illustrates that individuals in the Diet and Exercise intervention
1447 are highly represented by the LV3 pattern. (G) Scatter plot showing significant modules identified
1448 with SGEA. Seven gene ontology (GO) terms were associated with top-ranked genes, defined as
1449 those most strongly correlated with the LV3 brain loadings, with an area under the curve > 0.5 and
1450 $P < 0.05$. The significant terms are: negative regulation of response to oxidative stress
1451 (GO:1902883), glucose homeostasis (GO:0042593), carbohydrate homeostasis (GO:0033500),

1452 cellular glucose homeostasis (GO:0001678), cellular response to hexose stimulus (GO:0071331),
1453 cellular response to glucose stimulus (GO:0071333), and positive regulation of fatty acid transport
1454 (GO:2000193). PLS: Partial Least Squares. SGEA: Spatial Gene Enrichment Analysis.
1455
1456
1457